Hamburger Beiträge
zur Angewandten Mathematik

Analysis and an Interior Point Approach for TV Image Reconstruction Problems on Smooth Surfaces

Marc Herrmann, Roland Herzog, Heiko Kröner, Stephan Schmidt, José Vidal

Nr. 2017-12
April 2017

Analysis and an Interior Point Approach for TV Image Reconstruction Problems on Smooth Surfaces*

Marc Herrmann†, Roland Herzog‡, Heiko Kröner§, Stephan Schmidt†, and José Vidal‡

Abstract. [Lai, Chan (Computer Vision and Image Understanding, 2011)] introduced an analog of the total variation image reconstruction approach [Rudin, Osher, Fatemi (Physica D, 1992)] for images on smooth surfaces. The problem is defined in terms of quantities intrinsic to the surface and it is therefore independent of the parametrization. In this paper, a rigorous analytical framework is developed for this model and its Fenchel predual. It is shown that the predual of the total variation problem is a quadratic optimization problem for the predual vector field $\boldsymbol{p} \in \boldsymbol{H}(\mathrm{div}; S)$ with pointwise inequality constraints on the surface. As in the flat case, $\boldsymbol{p}$ serves as an edge detector. A function space interior point method is proposed for the predual problem, which is discretized by conforming Raviart–Thomas finite elements on a triangulation of the surface. Well-posedness of the barrier problems is established. Numerical examples including denoising and inpainting problems with both gray-scale and color images on scanned 3D geometries of considerable complexity are presented.

Key words. total bounded variation, Fenchel predual problem, interior-point methods, image reconstruction, image denoising, image inpainting, surfaces

AMS subject classifications. 94A08, 92C55, 68U10, 49M29, 65K05

1. Introduction.

We consider the image reconstruction problem

$$\text{(1)} \qquad \begin{cases} \text{Minimize} & \dfrac{1}{2}\displaystyle\int_S |Ku - f|^2 \,\mathrm{d}s + \dfrac{\alpha}{2}\int_S |u|^2 \,\mathrm{d}s + \beta \int_S |\nabla u| \\ \text{over} & u \in BV(S) \end{cases}$$

where $S \subset \mathbb{R}^3$ is a smooth, compact, orientable and connected surface without boundary. $BV(S)$ denotes the space of functions of bounded variation on the surface S, and $\int_S |\nabla u|$ is

*This work was supported by DFG grants HE 6077/10–1 and SCHM 3248/2–1 within the Priority Program SPP 1962 (*Non-smooth and Complementarity-based Distributed Parameter Systems: Simulation and Hierarchical Optimization*), which is gratefully acknowledged.

†Julius-Maximilians-Universität Würzburg, Faculty of Mathematics and Computer Science, Lehrstuhl für Mathematik VI, Emil-Fischer-Straße 40, D–97074 Würzburg, Germany (MH: marc.herrmann@mathematik.uni-wuerzburg.de; STS: stephan.schmidt@mathematik.uni-wuerzburg.de, https://www.mathematik.uni-wuerzburg.de/~schmidt).

‡Technische Universität Chemnitz, Faculty of Mathematics, Professorship Numerical Mathematics (Partial Differential Equations), D–09107 Chemnitz, Germany (RH: roland.herzog@mathematik.tu-chemnitz.de, https://www.tu-chemnitz.de/herzog, JV: jose.vidal-nunez@mathematik.tu-chemnitz.de, https://www.tu-chemnitz.de/mathematik/part_dgl/people/vidal).

§University of Hamburg, Fachbereich Mathematik, Bundesstraße 55, D–20146 Hamburg, Germany (heiko.kroener@uni-hamburg.de).

the surface analog of the total-variation seminorm, both of which are introduced in section 2. Furthermore, the observed data $f \in L^2(S)$, parameters $\beta > 0$, $\alpha \geq 0$ and the observation operator $K \in \mathcal{L}(L^2(S))$ are given. By $K^* \in \mathcal{L}(L^2(S))$ we denote the Hilbert space adjoint of K. It will be shown that $BV(S) \hookrightarrow L^2(S)$ so that the integrals in (1) are well defined. We assume throughout that either $\alpha > 0$ holds, or else that K is injective and has closed range, i.e., there exists a constant $\gamma > 0$ such that $\|Ku\|_{L^2(S)} \geq \gamma \|u\|_{L^2(S)}$ for all $u \in L^2(S)$. This second case is equivalent to K^*K being a coercive operator in $\mathcal{L}(L^2(S))$; see for instance [27, Chapter A.2].

The motivation to study (1) goes back to the seminal work in [46], where the total variation (TV) seminorm $\int |Du|$ was proposed as a regularizing functional in image reconstruction. Due to the choice of norms in the fidelity and regularizations terms, problem (1) is also termed a TV–L^2 model. A large body of literature on this topic has emerged; see for instance [15, 16, 17, 48, 51] and the references therein. The operator K appearing in (1) expresses available a-priori knowledge about the relation between the image u to be reconstructed and the observed data f. Common examples include $K = \mathrm{id}$ for classical image denoising [46], $K =$ masking for inpainting problems [19, Chapter 6.5], $K =$ blur for deblurring problems [13, 23], and $K =$ coarsen for un-zooming problems [38].

The increasing interest in studying image processing problems *on surfaces* is due to its numerous applications, for instance, in computer vision [33], geophysics [32], and medical imaging [37]. This is accompanied by the ongoing development in 3D scanning, remote sensing and other data acquisition hardware. In the applications mentioned unavoidable sampling errors from the imaging equipment, or the need to compress large-scale images, e.g., for limited-bandwidth internet applications, are potential sources of noise, necessitating post processing. The predominant approach in surface image processing so far is based on extensions of the nonlinear, anisotropic diffusion method going back to [40]. In particular, we mention [3, 20, 21] for surface intrinsic concepts, and [8, 9, 39] for volume-based formulations. We also point out [7] who consider an extension of the Mumford–Shah image segmentation problem using the active contour method on surfaces, with a subsequent restoration phase on the segmented parts driven by linear isotropic diffusion.

As an alternative to diffusion driven image restoration our focus here is on problem (1), which was recently proposed in [35] as an analog of the TV–L^2 reconstruction model for images defined on smooth *surfaces*. One of the algorithms considered for its solution was Chambolle's projection method [15], based on the *formal* convex dual problem of (1). The intention of the present paper is to extend the work of [35] in several directions. We establish a rigorous relation between the primal and dual problems in appropriate function spaces. To be precise, we formulate the *predual* of (1), which is a quadratic convex problem (14) with pointwise bound constraints in $\boldsymbol{H}(\mathrm{div}; S)$, the analog on surfaces of the space of vector-valued L^2 functions whose divergence is likewise square integrable. The distinction between dual and predual problems is necessary due to $BV(S)$ being non-reflexive. A similar analysis has previously been pursued in [31] for the 'flat' case. Notice however that in [31] the BV seminorm is defined in a way which is *not* rotationally invariant but has the advantage of leading to pointwise simple bounds $-\beta\,\mathbf{1} \leq \boldsymbol{p} \leq \beta\,\mathbf{1}$ for the dual variable $\boldsymbol{p}$. This structure is particularly amenable

to numerical solution via a primal-dual active set method. By contrast, we propose to use an *interior-point method*, which deals nicely with pointwise *nonlinear* constraints of the form $|\boldsymbol{p}|_2 \leq \beta$ arising in the *coordinate free setting* that naturally comes with surfaces. We establish the well-posedness of the barrier approximations for positive barrier parameter and provide necessary and sufficient optimality conditions in function space. Another distinction from previous work is that we do not introduce additional regularization terms as in [31, Sect. 3], which would lift the predual problem to one in $\boldsymbol{H}^{1,2}(S;\mathbb{R}^2)$ but add artificial diffusion. The last difference concerns the type of discretization employed. While Cartesian grids are natural in 'flat' image processing tasks and lend themselves to finite difference approximations, surfaces are naturally *triangularized*, for instance by 3D scanner software. Based on the rigorous formulation of the predual problem we are led to choose a conforming finite element discretization of the space $\boldsymbol{H}(\mathrm{div};S)$ by the surface analog of (possibly higher-order) Raviart–Thomas finite element spaces introduced in [43]. Notice that in [35] piecewise linear Lagrangian finite elements were considered, which are also $\boldsymbol{H}(\mathrm{div};S)$ conforming but do not exhaust that space.

This paper is organized as follows. In section 2 we introduce the proper functional analytic framework for the discussion of (1) and its predual. In particular, we recall the definition of the spaces $BV(S)$ and $\boldsymbol{H}(\mathrm{div};S)$ on a smooth surface S. Section 3 is devoted to the study of the Fenchel predual problem. In section 4 we formulate a function space interior point approach for the solution of the predual problem, analyze the well-posedness of the barrier approximations, and provide necessary and sufficient optimality conditions. Details concerning the discretization by Raviart–Thomas surface finite elements and the implementation of our method are also given in that section. Subsequently, numerical results are presented in section 5. While the presentation focuses on scalar (gray-scale) image data, an extension to multi-channel (color) images is rather straightforward and is presented, along with numerical results for denoising and inpainting problems, likewise in that section. We end with conclusions and an outlook in section 6.

2. Functional Analytic Framework.

In this section we introduce the necessary analytical framework to extend the definition of functions of bounded variation (BV) as well as functions in $\boldsymbol{H}(\mathrm{div})$ on an open subset of $\mathbb{R}^n$ to functions defined on smooth surfaces.

2.1. Concepts from Differential Geometry.

In a nutshell, a *smooth surface* S is a two-dimensional manifold of class C^∞ embedded in $\mathbb{R}^3$. In the interest of keeping the paper self-contained, we briefly summarize the required concepts from differential geometry. The interested reader is referred, for instance, to [22, 34, 41] for further background material.

Definition 1. *A subset $S \subset \mathbb{R}^3$, endowed with the relative topology of $\mathbb{R}^3$, is a* smooth surface *if for every point $p \in S$ there exists an open set $V \subset S$ containing p, an open set $U \subset \mathbb{R}^2$ and a homeomorphism $x : U \to V$ with the additional properties that $x \in C^\infty(U;\mathbb{R}^3)$ holds and that the Jacobian of x has rank 2 on U.*

A mapping x as above is called a *parametrization* at p. A collection of parametrizations covering all of S is said to be an *atlas* of S. We will always associate with a smooth surface an

atlas of parametrizations, and it will not matter throughout the paper which particular atlas is being used.

A function $f : S \to \mathbb{R}$ is said to be of *class* C^k if, for any parametrization x in the atlas, the function $f \circ x : U \subset \mathbb{R}^2 \to \mathbb{R}$ is of class C^k. Similarly, this notion can be defined for functions f defined only on an open subset of S by appropriately restricting those parametrizations whose image intersects the domain of definition of f.

We continue with the notions of tangent vectors and the tangent space at a point $p \in S$. Consider a differentiable curve $\gamma : (-\varepsilon, \varepsilon) \to S$ such that $\gamma(0) = p$. Then $X := \dot\gamma(0) \in \mathbb{R}^3$ is said to be the *tangent vector* to the curve γ at p. The *tangent space* at p, denoted by $T_p(S)$, consists of all tangent vectors of such curves γ at p. It is a vector space of dimension 2. If p belongs to the image of some parametrization x, then it is easy to verify that $\left\{ \frac{\partial x}{\partial u_1}(x^{-1}(p)), \frac{\partial x}{\partial u_2}(x^{-1}(p)) \right\}$ constitutes a basis for $T_p(S)$. Therefore, any tangent vector X at p can be represented as $X = X^i \frac{\partial x}{\partial u_i}(x^{-1}(p))$. Here and in the sequel we use Einstein's summation convention. The coefficients X^i are the *components* of the tangent vector $X \in T_p(S)$ in the local basis induced by the parametrization x.

The *tangent bundle* of S (as a set) is defined as $T(S) := \bigcup_{p\in S} \{p\} \times T_p(S)$. A (tangential) *vector field*[1] of class C^k $(k \geq 0)$ is a map $\boldsymbol{X} : S \to T(S)$ with the following properties:

(*i*) $\boldsymbol{X}(p) \in \{p\} \times T_p(S)$ for all $p \in S$, i.e., $\boldsymbol{X}$ is a *section*.

(*ii*) For any parametrization $x : U \to V$, the component functions $p \mapsto X^i(p)$ in the representation

$$\boldsymbol{X}(p) = X^i(p) \, \frac{\partial x}{\partial u_i}(x^{-1}(p)), \quad p \in V \tag{2}$$

are of class C^k on V.

Finally we recall the notion of *divergence* of a C^k vector field $\boldsymbol{X}$ for $k \geq 1$. Suppose that $\boldsymbol{X}$ has the representation (2) w.r.t. the parametrization x. Define the differential operators $(\partial_i \cdot)(p)$, $i = 1, 2$, by

$$(\partial_i f)(p) := \frac{\partial (f \circ x)}{\partial u_i}(x^{-1}(p))$$

for C^1 functions f defined in a neighborhood of $p \in S$. Following [45, Chapter 1.2.3], we have

$$(\operatorname{div} \boldsymbol{X})(p) := \frac{1}{\sqrt{\det G(p)}} \, \partial_i \left(X^i \sqrt{\det G} \right)(p), \quad p \in V. \tag{3}$$

Here G is the *metric tensor* for the parametrization x at p, defined by its entries

$$(g_{ij})(p) := \left(\frac{\partial x}{\partial u_i}(x^{-1}(p)) \right)^\top \left(\frac{\partial x}{\partial u_j}(x^{-1}(p)) \right), \quad p \in V,$$

[1] Vector fields on the surface and their corresponding function spaces will be denoted by bold-face symbols.

where $a^\top b$ denotes the Euclidean inner product in the ambient space $\mathbb{R}^3$. Since the vectors $\frac{\partial x}{\partial u_i}(x^{-1}(p))$, $i = 1, 2$ are linearly independent, $G(p)$ is positive definite and also symmetric.

Due to the fact that every tangent space to a point p on the surface inherits the standard inner product from the ambient space $\mathbb{R}^3$, we can introduce the *pointwise inner product* of two C^k vector fields as $(\boldsymbol{X}, \boldsymbol{Y})_2 := \boldsymbol{X}^\top \boldsymbol{Y}$, resulting in a real-valued C^k function on S. Moreover, the *pointwise 2-norm* of a vector field will be denoted by $|\boldsymbol{X}|_2 = (\boldsymbol{X}, \boldsymbol{X})_2^{1/2}$. When $\boldsymbol{X}$ and $\boldsymbol{Y}$ are given by representations of type (2) w.r.t. a parametrization x, then the product $(\boldsymbol{X}, \boldsymbol{Y})_2$ is represented by $g_{ij} X^i Y^j$. Notice that the notions of tangent space, tangent bundle, vector fields and their divergence, as well as the inner product $(\cdot, \cdot)_2$ and the norm $|\cdot|_2$ are intrinsic quantities, i.e., independent of the atlas used to describe the surface S.

Assumption 2. *Throughout this paper we will assume that the smooth surface $S \subset \mathbb{R}^3$ is compact and connected.*

It can be shown that for smooth surfaces, connectedness implies that any two points can be joined by a smooth path. As a further consequence of Assumption 2 S is also *orientable*; cf. [2, Prob. 2.43]. That is, the Jacobian of the transition map $x^{-1} \circ y$ between any two intersecting parametrizations has positive determinant on its domain of definition.

2.2. Sobolev Functions and Functions of Bounded Variation. In this section we recall the notions of Lebesgue and Sobolev spaces $L^p(S)$ and $H^{1,p}(S)$ on the surface S, as well as the spaces $\boldsymbol{H}(\mathrm{div}; S)$ and $BV(S)$ required for the subsequent analysis.

For $m \in \mathbb{N}_0$, $C^m(S)$ denotes the space of C^m functions on the surface S. Moreover, $\boldsymbol{C}^m(S; T(S))$ denotes the space of C^m vector fields. As usual, the support of a function f is defined as

$$\operatorname{supp} f := \operatorname{cl}\{p \in S : f(p) \neq 0\}$$

with $\operatorname{cl} C$ denoting the *closure* of a set $C \subset S$.

We begin with the recollection of the spaces $L^p(S)$. Let f be a continuous function on S with support in the range V of a parametrization $x : U \to V$. Then, we have by definition

$$\int_S f \,\mathrm{d}s := \int_U f(x(u)) \sqrt{\det G(x(u))}\,\mathrm{d}u,$$

where the measure $\mathrm{d}s$ is defined as $\mathrm{d}s = \sqrt{(\det G) \circ x}\,\mathrm{d}u$, with $\mathrm{d}u$ denoting the Lebesgue measure in $\mathbb{R}^2$. This definition of the integral extends to arbitrary continuous functions on S by using a partition of unity; cf. [29, Ch. 1.2]. As it is shown there the integrability of a function and the value of its integral over S depend neither on the atlas nor on the partition of unity used.

For $1 \leq p < \infty$ the space $L^p(S)$ is defined as the completion of $C^\infty(S)$ w.r.t. the norm

$$\|f\|_{L^p(S)} := \left(\int_S |f|^p \,\mathrm{d}s \right)^{1/p}. \tag{4}$$

We also recall that $L^\infty(S)$ is defined as the space of functions such that

$$\|f\|_{L^\infty(S)} := \operatorname*{ess\,sup}_{p\in S} |f(p)| < \infty.$$

Naturally, these definitions extend to vector fields $\boldsymbol{f} \in \boldsymbol{L}^p(S;T(S))$. For instance, we have

$$\|\boldsymbol{f}\|_{\boldsymbol{L}^p(S;T(S))} := \left(\int_S |\boldsymbol{f}|_2^p \,\mathrm{d}s\right)^{1/p}.$$

The spaces $L^2(S)$ and $\boldsymbol{L}^2(S;T(S))$ are Hilbert spaces w.r.t. the usual inner products $(\cdot,\cdot)_{L^2(S)}$ and $(\cdot,\cdot)_{\boldsymbol{L}^2(S;T(S))}$.

We are now in the position to define functions of bounded variation on surfaces satisfying Assumption 2. Background material on BV functions on flat domains can be found, for instance, in [26], [53, Ch. 5] or [1, Ch. 10].

Definition 3 (see also [35, Sect. 3.1] or [6, Sect. 4]). *A function $u \in L^1(S)$ belongs to $BV(S)$ if the TV-seminorm defined by*

$$\int_S |\nabla u| := \sup\left\{\int_S u \operatorname{div} \boldsymbol{\eta}\,\mathrm{d}s : \boldsymbol{\eta} \in \boldsymbol{V}\right\} \tag{5}$$

is finite, where

$$\boldsymbol{V} := \{\boldsymbol{\eta} \in \boldsymbol{C}^\infty(S;T(S)) : |\boldsymbol{\eta}(p)|_2 \le 1 \text{ for all } p \in S\}.$$

We equip the space $BV(S)$ with the norm

$$\|u\|_{BV(S)} = \|u\|_{L^1(S)} + \int_S |\nabla u|, \quad u \in BV(S). \tag{6}$$

It is worth remarking that, as in the planar case, $\int_S |\nabla u| = \int_S |\nabla u|\,\mathrm{d}s$ holds for all functions $u \in C^\infty(S)$ and indeed for $u \in H^{1,1}(S)$; see [45, p.18] and Definition 4 below. Notice that both contributions to the norm $\|\cdot\|_{BV(S)}$ are independent of the parametrization. We also remark that the space $\boldsymbol{C}^\infty(S;T(S))$ can be replaced by $\boldsymbol{C}^1(S;T(S))$ without affecting the definition; compare [1, Def. 10.1.1], [53, p.221] or [6].

According to Definition 3, it is clear that the embedding $BV(S) \hookrightarrow L^1(S)$ holds. Next, we are going to prove that even $BV(S) \hookrightarrow L^2(S)$ is valid, as is known for two-dimensional flat domains; see for instance [1, Th. 10.1.3]. This result is essential to establish the well-posedness of (1) in the sequel. Its proof requires the notion of intermediate convergence of $BV(S)$ functions as well as the concept of first-order Sobolev spaces $H^{1,p}(S)$. We summarize only the essential concepts and refer the reader to [28, 29] for an in-depth introduction to Sobolev spaces on manifolds.

Definition 4. *Let $u \in C^\infty(S)$. We call $\nabla u : S \to \mathbb{R}^3$ the* gradient*, defined locally in terms of any parametrization x by*

$$\nabla u := g^{ij}\,(\partial_i u)\,\frac{\partial x}{\partial u_j}.$$

The gradient assigns to each point $p \in S$ a vector $(\nabla u)(p)$ in $T_p(S) \subset \mathbb{R}^3$ verifying

$$\big((\nabla u)(p),\, v\big)_2 = v^i(\partial_i u)(p)$$

for all $v = v^i \frac{\partial x}{\partial u_i}(x^{-1}(p)) \in T_p(S)$. Here, g^{ij} are the components of the inverse *of the metric tensor $G = (g_{ij})$. Furthermore, we define*

$$|\nabla u|_2 := \left(g^{ij}(\partial_i u)(\partial_j u)\right)^{1/2}.$$

Now for $1 \le p < \infty$ and a function $u \in C^\infty(S)$, define the norm

$$\|u\|_{H^{1,p}(S)} := \left(\|u\|^p_{L^p(S)} + \int_S |\nabla u|_2^p \,\mathrm{d}s\right)^{1/p}. \tag{7}$$

The Sobolev space $H^{1,p}(S)$ is then given by

$$H^{1,p}(S) := \mathrm{cl}\,(C^\infty(S))$$

where the closure is w.r.t. the norm (7).

The counterpart of the following definition in the classical framework can be found in [1, Definition 10.1.3].

Definition 5. *Let $\{u_n\}$ be a sequence of functions in $BV(S)$ and suppose $u \in BV(S)$. We say that $u_n \to u$ in the sense of* intermediate convergence *if*

(*i*) *$u_n \to u$ strongly in $L^1(S)$ and*

(*ii*) $\displaystyle\int_S |\nabla u_n| \to \int_S |\nabla u|.$

The following lemma can be proved analogously as in [1, Th. 10.1.2]. The proof uses a partition-of-unity argument as well as mollification.

Lemma 6. *For any $u \in BV(S)$, there exists a sequence $\{u_k\} \subset C^\infty(S)$ with $u_k \to u$ in the intermediate sense.*

Proposition 7. *The space $BV(S)$, equipped with the norm (6), is a Banach space and the embedding*

$$BV(S) \hookrightarrow L^p(S)$$

holds for all $1 \le p \le 2$.

Proof. The first part of the claim can be shown along the lines of [1, Prop. 10.1.1, Th. 10.1.1] taking into consideration the definition of the $\|\cdot\|_{L^p(S)}$ given in (4). Hence, let us focus on the proof of the second claim. To this aim, let us define $\{u_n\} \subset C^\infty(S)$ which converges to $u \in BV(S)$ in the sense of intermediate convergence. Due to [29, Th. 2.6], we have that the embedding $H^{1,q}(S) \hookrightarrow L^p(S)$ is continuous for all $q \in [1,2)$ and $p = \frac{2q}{2-q}$. In particular, for $q = 1$ and $p = 2$ we have $H^{1,1}(S) \hookrightarrow L^2(S)$, so there exists $c > 0$ such that

$$\left(\int_S |u_n|^2 \,\mathrm{d}s\right)^{1/2} \leq c\left(\int_S |u_n| \,\mathrm{d}s + \int_S |\nabla u_n|_2 \,\mathrm{d}s\right)$$

since $\{u_n\} \subset C^\infty(S) \subset H^{1,1}(S)$. Hence,

$$\begin{aligned}\left(\int_S |u|^2 \,\mathrm{d}s\right)^{1/2} &= \left(\int_S \lim_{n\to\infty} |u_n|^2 \,\mathrm{d}s\right)^{1/2} \leq \liminf_{n\to\infty}\left(\int_S |u_n|^2 \,\mathrm{d}s\right)^{1/2} \\ &\leq \liminf_{n\to\infty} c\left(\int_S |u_n| \,\mathrm{d}s + \int_S |\nabla u_n|_2 \,\mathrm{d}s\right) \\ &= c\left(\|u\|_{L^1(S)} + \int_S |\nabla u|\right) = c\,\|u\|_{BV(S)}.\end{aligned}$$

Then, applying [29, Cor. 2.1], we have that $BV(S) \hookrightarrow L^p(S)$ holds for all $p \in [1,2]$. ∎

To close this section we introduce the following space of vector fields, which will play a fundamental role throughout the paper,

$$\boldsymbol{H}(\mathrm{div}; S) := \left\{\boldsymbol{v} \in \boldsymbol{L}^2(S; T(S)) : \mathrm{div}\,\boldsymbol{v} \in L^2(S)\right\}.$$

We equip this space with the norm

$$\|\boldsymbol{v}\|_{\boldsymbol{H}(\mathrm{div};S)} := \left(\|\boldsymbol{v}\|^2_{\boldsymbol{L}^2(S;T(S))} + \|\mathrm{div}\,\boldsymbol{v}\|^2_{L^2(S)}\right)^{1/2}, \tag{8}$$

which is induced by the inner product

$$(\boldsymbol{v}, \boldsymbol{w})_{\boldsymbol{H}(\mathrm{div};S)} := (\boldsymbol{v}, \boldsymbol{w})_{\boldsymbol{L}^2(S;T(S))} + (\mathrm{div}\,\boldsymbol{v}, \mathrm{div}\,\boldsymbol{w})_{L^2(S)}.$$

$\boldsymbol{H}(\mathrm{div}; S)$ is a Hilbert space.

3. The Fenchel Predual on Surfaces. The dual problem of TV–L^2 has been stated in various references; see for instance [14, 15, 18]. In particular, it appears in [35] exactly for problem (1) on smooth surfaces. However, the arguments used to derive the dual problem in these references were all *formal*, and in particular no function space was assigned to the problem. To the best of our knowledge [31] is the only reference where this analysis is made rigorous. Due to the lack of reflexivity of BV spaces, the dual and predual problems are different. As has been shown in [31] the *predual*, posed as a problem in $\boldsymbol{H}(\mathrm{div})$, is the appropriate concept.

In this section we adapt this rigorous analysis to problem (1) on the surface S. As expected from [35] the predual problem is a quadratic optimization problem for the predual tangent field $\boldsymbol{p} \in \boldsymbol{H}(\mathrm{div}; S)$ with pointwise constraints on the surface; see (14) below. We will show that both problems are equivalent and that the primal solution can be recovered from the predual solution. We wish to point out that the constraints $|\boldsymbol{p}|_2 \leq \beta$ arising in our setting are nonlinear. This is in contrast with [31, eq. (2.1)], where simple bounds $-\beta\,\mathbf{1} \leq \boldsymbol{p} \leq \beta\,\mathbf{1}$ were obtained due to a slightly different definition of the TV-seminorm, which is, however, not invariant under changes of the parametrization.

Solving the predual problem has a number of advantages compared to solving the primal problem directly. First, we do not have to deal with the discretization of the nonsmooth term $\int_S |\nabla u|$ in the finite element context, nor employ an optimization algorithm for the nonsmooth problem (1); we mention however that such a program was carried out in a different context in [4]. Second, as was pointed out in [5], the finite element solution of minimization problems in BV spaces may suffer from low convergence rates. Finally, as was observed previously in [14, 15, 18, 31], we mention that the predual variable $\boldsymbol{p}$ serves as an edge detector in the image.

Let us recall some preliminary results from convex analysis; see for instance [52, Ch. 2.8]. Given two locally convex Hausdorff spaces X, Y, two proper convex functions $F : X \to \mathbb{R} \cup \{\infty\}$, $G : Y \to \mathbb{R} \cup \{\infty\}$ as well as a bounded linear map $A : X \to Y$ we have, due to the Fenchel-Young inequality, the relation of weak duality

$$\inf_{x \in X} \{F(x) + G(Ax)\} \geq \sup_{y^* \in Y^*} \{-F^*(A^* y^*) - G^*(-y^*)\}\,. \tag{9}$$

Here $F^* : X^* \to \mathbb{R}$ and $G^* : Y^* \to \mathbb{R}$ are the Fenchel conjugates of F and G, defined by

$$F^*(x^*) = \sup_{x \in X} \{\langle x,\, x^* \rangle - F(x)\} \quad \text{and} \quad G^*(y^*) = \sup_{y \in Y} \{\langle y,\, y^* \rangle - G(y)\} \tag{10}$$

and X^* and Y^* are the topological dual spaces of X and Y. Moreover $A^* : Y^* \to X^*$ stands for the adjoint operator of A. Under the assumption

$$A(\mathrm{dom}\, F) \cap \{y \in Y : G \text{ is continuous in } y\} \neq \emptyset \tag{11}$$

strong Fenchel duality holds, i.e.,

$$\inf_{x \in X} \{F(x) + G(Ax)\} = \max_{y^* \in Y^*} \{-F^*(A^* y^*) - G^*(-y^*)\}\,. \tag{12}$$

We now apply this to our specific setting. As in [31] we define the operator B as

$$B := \alpha\,\mathrm{id} + K^* K \in \mathcal{L}(L^2(S)), \tag{13}$$

where id is the identity mapping. Furthermore, we define

$$\|w\|^2_{B^{-1}} = (w, B^{-1} w)_{L^2(S)} = (w, w)_{B^{-1}}$$

for any $w \in L^2(S)$. Notice that in view of our standing assumptions ($\alpha > 0$ or K^*K coercive), $\|w\|_{B^{-1}}$ is a norm equivalent to the standard norm of $L^2(S)$.

Theorem 8. *The Fenchel dual problem of*

$$\text{(14)}\qquad \begin{cases} \text{Minimize} & \frac{1}{2}\|\operatorname{div} \boldsymbol{p} + K^* f\|^2_{B^{-1}} \\ \text{over} & \boldsymbol{p} \in \boldsymbol{H}(\operatorname{div}; S) \\ \text{subject to} & |\boldsymbol{p}|_2 \le \beta \quad \text{a.e. on } S \end{cases}$$

is equivalent to the optimization problem (1). *In other words,* (14) *can be seen as the predual of the primal problem* (1).

Proof. The proof proceeds along the lines of [31, Th. 2.2]. We invoke the Fenchel duality theory in the setting $X = \boldsymbol{H}(\operatorname{div}; S)$, $Y = L^2(S)$ and $A = -\operatorname{div} : X \to Y$. It is convenient to identify Y with Y^* so that $A^* = -\operatorname{div}^* : Y \to X^*$. Define the functions $F : \boldsymbol{H}(\operatorname{div}; S) \to \mathbb{R}$ and $G : L^2(S) \to \mathbb{R}$ as

$$\text{(15)}\qquad \begin{aligned} F(\boldsymbol{p}) &:= \begin{cases} 0 & \text{if } |\boldsymbol{p}|_2 \le \beta \text{ a.e. on } S, \\ \infty & \text{otherwise,} \end{cases} \\ G(v) &:= \frac{1}{2}\|v - K^* f\|^2_{B^{-1}}. \end{aligned}$$

From [31] we have

$$\text{(16)}\qquad G^*(v^*) = \sup_{v \in L^2(S)} \left\{ (v, v^*)_{L^2(S)} - G(v) \right\} = \frac{1}{2}\|Kv^* + f\|^2_{L^2(S)} + \frac{\alpha}{2}\|v^*\|^2_{L^2(S)} - \frac{1}{2}\|f\|^2_{L^2(S)}$$

for $v^* \in L^2(S)$. With regard to $F^* : \boldsymbol{H}(\operatorname{div}; S)^* \to \mathbb{R}$ it is clear that

$$F^*(\boldsymbol{p}^*) = \sup_{\boldsymbol{p} \in \mathcal{B}_0} \langle \boldsymbol{p}, \boldsymbol{p}^* \rangle_{\boldsymbol{H}(\operatorname{div};S), \boldsymbol{H}(\operatorname{div};S)^*}$$

holds, where

$$\mathcal{B}_0 := \{ \boldsymbol{p} \in \boldsymbol{H}(\operatorname{div}; S) : |\boldsymbol{p}|_2 \le \beta \text{ a.e. on } S \}.$$

It can be shown by a projection argument that the set

$$\mathcal{B}_1 := \{ \boldsymbol{p} \in \boldsymbol{C}^\infty(S; T(S)) : |\boldsymbol{p}|_2 \le \beta \text{ a.e. on } S \}$$

is dense in $\mathcal{B}_0$ in the topology of $\boldsymbol{H}(\operatorname{div}; S)$. Hence, for every $u \in L^2(S)$ we obtain

$$\begin{aligned} F^*((-\operatorname{div})^* u) &= \sup\{ \langle \boldsymbol{p}, (-\operatorname{div})^* u \rangle_{\boldsymbol{H}(\operatorname{div};S), \boldsymbol{H}(\operatorname{div};S)^*} : \boldsymbol{p} \in \mathcal{B}_1 \} \\ &= \sup\{ (u, -\operatorname{div} \boldsymbol{p})_{L^2(S)} : \boldsymbol{p} \in \mathcal{B}_1 \} \\ &= \beta \sup\{ (u, \operatorname{div} \boldsymbol{p})_{L^2(S)} : \boldsymbol{p} \in \boldsymbol{C}^\infty(S; T(S)) : |\boldsymbol{p}|_2 \le 1 \text{ a.e. on } S \}. \end{aligned}$$

Therefore according to Definition 3 we get

$$\text{(17)}\qquad F^*((-\operatorname{div})^* u) = \begin{cases} \beta \displaystyle\int_S |\nabla u| & \text{if } u \in BV(S), \\ \infty & \text{otherwise.} \end{cases}$$

Thus, since F and G are proper and convex and condition (11) is fulfilled for them, there is no duality gap between the optimal values of (1) and (14), i.e., (9) becomes an equality and

$$\begin{aligned}
&\inf_{\boldsymbol{p}\in\boldsymbol{H}(\mathrm{div};S)} \{F(\boldsymbol{p}) + G(-\operatorname{div}\boldsymbol{p})\} \\
&\quad = \sup_{u\in L^2(S)} \{-F^*((-\operatorname{div})^* u) - G^*(-u)\} \\
&\quad = \sup_{u\in BV(S)} \{-F^*((-\operatorname{div})^* u) - G^*(-u)\} \\
&\quad = \sup_{u\in BV(S)} \left\{-\frac{1}{2}\|Ku - f\|^2_{L^2(S)} - \frac{\alpha}{2}\|u\|^2_{L^2(S)} - \beta \int_S |\nabla u|\right\} + \frac{1}{2}\|f\|^2_{L^2(S)}. \qquad (18)
\end{aligned}$$

Finally, it is immediate to check that (18) is in turn equivalent to (1) . ∎

Corollary 9. *Problem* (1) *and its predual* (14) *are solvable.*

Proof. The existence of a solution to (14) follows from standard arguments using the direct method of the calculus of variations and the embedding $BV(S) \hookrightarrow L^2(S)$ proved in Proposition 7. We refer the reader to the proof of Proposition 11 for details, where the same arguments are applied to a variation of (14). Regarding the solvability of (1), since condition (11) is fulfilled for F and G defined in the proof of Theorem 8, we conclude that the supremum in the RHS of (18) is attained, so (12) holds and the optimization problem (1) is solvable. ∎

The following theorem shows how the optimal solutions to (1) and (14) are related to each other.

Theorem 10. *Suppose that* $\overline{\boldsymbol{p}}$ *is an optimal solution to* (14) *and* $\overline{u}$ *is optimal to* (1). *Then*

$$B\,\overline{u} = \operatorname{div}\overline{\boldsymbol{p}} + K^* f. \qquad (19)$$

Proof. Suppose that $\overline{\boldsymbol{p}}$ and $\overline{u}$ are optimal to (14) and (1), respectively. Then the following conditions are fulfilled, see for instance [25, Prop. 4.1],

$$\begin{aligned}
(-\operatorname{div})^*\overline{u} &\in \partial F(\overline{\boldsymbol{p}}) \qquad \text{in } \boldsymbol{H}(\mathrm{div};S)^*, \\
-\operatorname{div}\overline{\boldsymbol{p}} &\in \partial G^*(-\overline{u}) \quad \text{in } L^2(S),
\end{aligned} \qquad (20)$$

where ∂F stands for the standard representation of the subdifferential of the convex function $F : \boldsymbol{H}(\mathrm{div};S) \to \mathbb{R}$, and ∂G^* is defined analogously. The second condition in (20) is equivalent to

$$G^*(-\overline{u}) + G(-\operatorname{div}\overline{\boldsymbol{p}}) - (-\operatorname{div}\overline{\boldsymbol{p}}, -\overline{u})_{L^2(S)} = 0.$$

Using the expressions (15) and (16) for G and G^*, this becomes

$$\frac{1}{2}\|K(-\overline{u}) + f\|^2_{L^2(S)} + \frac{\alpha}{2}\|\overline{u}\|^2_{L^2(S)} - \frac{1}{2}\|f\|^2_{L^2(S)} + \frac{1}{2}\|\operatorname{div}\overline{\boldsymbol{p}} + K^* f\|^2_{B^{-1}} = (\operatorname{div}\overline{\boldsymbol{p}}, \overline{u})_{L^2(S)},$$

or equivalently,

$$\frac{1}{2}\|K\overline{u}\|^2_{L^2(S)} + \frac{\alpha}{2}\|\overline{u}\|^2_{L^2(S)} + \frac{1}{2}\|\operatorname{div}\overline{\boldsymbol{p}} + K^* f\|^2_{B^{-1}} = (\operatorname{div}\overline{\boldsymbol{p}} + K^* f, \overline{u})_{L^2(S)}.$$

Applying the definition of B, see (13), we obtain

$$\frac{1}{2}\left\|u - B^{-1}(\operatorname{div}\overline{\boldsymbol{p}} + K^* f)\right\|_B^2 = 0$$

and (19) follows. ∎

4. Algorithmic Approach and Finite Element Discretization. In this section we describe a novel approach for solving (1) via its predual (14). Once again, recall that the pointwise constraints $|\boldsymbol{p}|_2 \leq \beta$ are nonlinear. This is in contrast with $|\boldsymbol{p}|_\infty \leq \beta$ obtained in [31] due to a slightly different definition of the TV-seminorm. The nonlinearity of the constraint would render the analysis and application of a primal-dual active set method more challenging although this has been successfully pursued, for instance, in [30, 50] in different contexts.

Our solution approach is based on a logarithmic barrier method to deal with the inequality constraints. Consequently, we consider the following family of convex problems for a decreasing sequence of barrier parameters $\mu \searrow 0$:

$$\left\{\begin{array}{rl} \text{Minimize} & \dfrac{1}{2}\|\operatorname{div}\boldsymbol{p} + K^* f\|_{B^{-1}}^2 - \mu \displaystyle\int_S \ln\left(\beta^2 - |\boldsymbol{p}|_2^2\right) \mathrm{d}s \\ \text{over} & \boldsymbol{p} \in \boldsymbol{H}(\operatorname{div}; S) \\ \text{subject to} & |\boldsymbol{p}|_2 \leq \beta \text{ a.e. on } S. \end{array}\right. \tag{21}$$

Notice that the constraint $|\boldsymbol{p}|_2 \leq \beta$ is explicitly kept in (21) for mathematical convenience and it avoids the need to define the logarithmic barrier term for negative arguments. For any fixed barrier parameter $\mu > 0$, problem (21) will be solved using Newton's method. The constraint $|\boldsymbol{p}|_2 \leq \beta$ is not enforced explicitly but its satisfaction will be monitored throughout the Newton iterations. More details concerning the implementation are given in section 5.

For convenience, we use the abbreviations

$$H(\boldsymbol{p}) := \frac{1}{2}\|\operatorname{div}\boldsymbol{p} + K^* f\|_{B^{-1}}^2 \quad \text{and} \quad b(\boldsymbol{p}) := -\mu \int_S \ln\left(\beta^2 - |\boldsymbol{p}|_2^2\right) \mathrm{d}s \tag{22}$$

in the sequel.

4.1. Existence and Uniqueness for the Predual Barrier Problem. The analysis of interior point methods in L^p spaces including a convergence analysis of the central path has been addressed in [42, 49] in the context of optimal control problems. Notice that the presence of the logarithmic barrier term helps to overcome the lack of strict convexity of the objective in (14). We therefore obtain the following result.

Proposition 11. *For every $\mu > 0$, problem (21) possesses a unique solution $\boldsymbol{p} \in \boldsymbol{H}(\operatorname{div}; S)$.*

Proof. It is easy to check that the objective $H(\boldsymbol{p}) + b(\boldsymbol{p})$ is bounded below by $b(\boldsymbol{0}) = -\mu\,(\operatorname{area} S)\,\ln(\beta^2)$ but it may attain the value ∞. Let us consider a minimizing sequence $\{\boldsymbol{p}_n\}$. Owing to the boundedness of both terms in the objective as well as $|\boldsymbol{p}_n|_2 \leq \beta$, $\{\boldsymbol{p}_n\}$ is

bounded in $\boldsymbol{H}(\operatorname{div}; S)$. Hence there exists a subsequence (again denoted by $\{\boldsymbol{p}_n\}$) such that $\boldsymbol{p}_n \rightharpoonup \overline{\boldsymbol{p}}$ in $\boldsymbol{L}^2(S; T(S))$ holds with $|\overline{\boldsymbol{p}}|_2 \le \beta$ a.e. on S, as well as $\operatorname{div} \boldsymbol{p}_n \rightharpoonup \operatorname{div} \boldsymbol{p}$ in $L^2(S)$.

By weak sequential lower semicontinuity of H,

$$H(\overline{\boldsymbol{p}}) = \frac{1}{2}\|\operatorname{div} \overline{\boldsymbol{p}} + K^* f\|_{B^{-1}}^2 \le \liminf_{n\to\infty} \frac{1}{2}\|\operatorname{div} \boldsymbol{p}_n + K^* f\|_{B^{-1}}^2$$

holds. Let us argue that b is also weakly sequentially lower semicontinuous w.r.t. $\boldsymbol{L}^2(S; T(S))$. To this end, it suffices to show that b is sequentially lower semicontinuous w.r.t. the strong topology of $\boldsymbol{L}^2(S; T(S))$ on

$$\mathcal{B} := \{\boldsymbol{q} \in \boldsymbol{L}^2(S; T(S)) : |\boldsymbol{q}|_2 \le \beta \text{ a.e. on } S\},$$

since $\mathcal{B}$ is closed and convex and b is convex in $\mathcal{B}$. Arguing similarly as in the proof of [49, Proposition 2], suppose that $\boldsymbol{q}_n \to \boldsymbol{q}$ in $\boldsymbol{L}^2(S; T(S))$ holds, where $\boldsymbol{q}_n \in \mathcal{B}$, and thus $\boldsymbol{q} \in \mathcal{B}$ holds as well. We have to show $b(\boldsymbol{q}) \le \liminf_{n\to\infty} b(\boldsymbol{q}_n)$, which is clear if the right hand side is ∞. In case $\liminf_{n\to\infty} b(\boldsymbol{q}_n) < \infty$, we can select a subsequence, denoted by $\{\boldsymbol{q}_j\}$, such that

$$\lim_{j\to\infty} b(\boldsymbol{q}_j) = \liminf_{n\to\infty} b(\boldsymbol{q}_n) \quad \text{and} \quad \boldsymbol{q}_j \xrightarrow{j\to\infty} \boldsymbol{q} \text{ a.e. on } S.$$

In particular, $b(\boldsymbol{q}_j) \le C$ holds for all j.

Let us define

$$\begin{aligned} g_n &:= -\mu \ln \max\{\beta^2 - |\boldsymbol{q}_n|_2^2,\ 1\}, \quad h_n := -\mu \ln \min\{\beta^2 - |\boldsymbol{q}_n|_2^2,\ 1\}, \\ g &:= -\mu \ln \max\{\beta^2 - |\boldsymbol{q}|_2^2,\ 1\}, \qquad h := -\mu \ln \min\{\beta^2 - |\boldsymbol{q}|_2^2,\ 1\}. \end{aligned}$$

Since $x \mapsto \ln x$ is Lipschitz continuous with Lipschitz constant 1 on $[1, \infty)$, we have

$$|g_n - g| \le \mu \left|\max\{\beta^2 - |\boldsymbol{q}_n|_2^2,\ 1\} - \max\{\beta^2 - |\boldsymbol{q}|_2^2,\ 1\}\right| \le \mu \left||\boldsymbol{q}_n|_2^2 - |\boldsymbol{q}|_2^2\right| \le \mu\, \beta^2$$

holds. Notice that $\lim_{j\to\infty} \boldsymbol{q}_j = \boldsymbol{q}$ a.e. on S implies $\lim_{j\to\infty} g_j = g$ and $\lim_{j\to\infty} h_j = h$ a.e. on S. Hence Lebesgue's dominated convergence theorem implies

$$\lim_{j\to\infty} \int_S g_j \,\mathrm{d}s = \int_S g \,\mathrm{d}s.$$

Consequently,

$$\lim_{j\to\infty} \int_S h_j \,\mathrm{d}s = \lim_{j\to\infty} b(\boldsymbol{q}_j) - \lim_{j\to\infty} \int_S g_j \,\mathrm{d}s$$

exists as well.

Using $h_n \ge 0$ and $|g_n| \le \mu \left||\boldsymbol{q}_n|_2^2 - \beta^2 + 1\right|$, we obtain

$$0 \le \int_S h_j \,\mathrm{d}s \le C - \int_S g_j \,\mathrm{d}s \le C + \mu \int_S \left||\boldsymbol{q}_j|_2^2 - \beta^2 + 1\right| \mathrm{d}s \le C + C'$$

for all j. By Fatou's lemma, we thus conclude

$$0 \le \int_S h \,\mathrm{d}s = \int_S \lim_{j\to\infty} h_j \,\mathrm{d}s \le \lim_{j\to\infty} \int_S h_j \,\mathrm{d}s \le C + C'.$$

This implies

$$\liminf_{n\to\infty} \int_S (g_n + h_n)\,\mathrm{d}s = \liminf_{n\to\infty} b(\boldsymbol{q}_n) = \lim_{j\to\infty} b(\boldsymbol{q}_j) \ge \int_S (g+h)\,\mathrm{d}s = b(\boldsymbol{q}).$$

Consequently, both summands H and b in the objective are weakly sequentially lower semicontinuous, which implies that $\overline{\boldsymbol{p}}$ is a (global) minimizer of (21).

To show its uniqueness, we verify that the second part of the objective b is strictly convex where it is finite. To this end, let $\boldsymbol{p}_1$ and $\boldsymbol{p}_2$ be two elements of $\mathcal{B}$ where $b(\boldsymbol{p}_1), b(\boldsymbol{p}_2) < \infty$ and $\boldsymbol{p}_1$ not equal to $\boldsymbol{p}_2$ a.e. on S. Then by classical arguments there exists a set $E \subset S$ of positive surface measure and $\varepsilon > 0$ such that $|\boldsymbol{p}_1 - \boldsymbol{p}_2|_2 \ge \varepsilon$ a.e. on E.

Let us define $g(\boldsymbol{p}) := |\boldsymbol{p}|_2^2$ and $h(z) := -\mu \ln(\beta^2 - z)$, whence $b(\boldsymbol{p}) = \int_S h(g(\boldsymbol{p}))\,\mathrm{d}s$ holds. On the set E, we have the following pointwise estimate due to the strong convexity of g,

$$(*) \quad g\big(\lambda\,\boldsymbol{p}_1 + (1-\lambda)\,\boldsymbol{p}_2\big) - \lambda\, g(\boldsymbol{p}_1) - (1-\lambda)\, g(\boldsymbol{p}_2) = -\lambda\,(1-\lambda)\,|\boldsymbol{p}_1 - \boldsymbol{p}_2|_2^2 \le -\lambda\,(1-\lambda)\,\varepsilon^2$$

for all $\lambda \in [0,1]$. Next we use that h is convex and strictly increasing on $[0,\beta^2)$. Its minimal slope is attained at $z = 0$ so we have $h'(z) \ge h'(0) = \mu/\beta^2$ for all $z \in [0,\beta^2)$. Consequently, we have $h(r) \ge h(\ell) + h'(\ell)(r-\ell) \ge h(\ell) + h'(0)(r-\ell)$ for all $0 \le \ell \le r < \beta^2$. Applying this estimate with $\ell = g\big(\lambda\,\boldsymbol{p}_1 + (1-\lambda)\,\boldsymbol{p}_2\big)$ and $r = \lambda\, g(\boldsymbol{p}_1) + (1-\lambda)\, g(\boldsymbol{p}_2)$ and using $(*)$, we obtain

$$h\Big(g\big(\lambda\,\boldsymbol{p}_1 + (1-\lambda)\,\boldsymbol{p}_2\big)\Big) \le h\Big(\lambda\, g(\boldsymbol{p}_1) + (1-\lambda)\, g(\boldsymbol{p}_2)\Big) - \frac{\mu}{\beta^2}\,\lambda\,(1-\lambda)\,\varepsilon^2.$$

Using the convexity of h we can estimate further

$$h\Big(g\big(\lambda\,\boldsymbol{p}_1 + (1-\lambda)\,\boldsymbol{p}_2\big)\Big) \le \lambda\, h\big(g(\boldsymbol{p}_1)\big) + (1-\lambda)\, h\big(g(\boldsymbol{p}_2)\big) - \frac{\mu}{\beta^2}\,\lambda\,(1-\lambda)\,\varepsilon^2,$$

which holds a.e. on E. Similarly, we obtain the same estimate without the last term on $S \setminus E$. Integrating these inequalities over S, we finally obtain the estimate

$$b\big(\lambda\,\boldsymbol{p}_1 + (1-\lambda)\,\boldsymbol{p}_2\big) \le \lambda\, b(\boldsymbol{p}_1) + (1-\lambda)\, b(\boldsymbol{p}_2) - \frac{\mu}{\beta^2}\,\lambda\,(1-\lambda)\,\varepsilon^2\,(\operatorname{area} E),$$

which confirms the strict convexity of b on its domain. ∎

Next we address the first-order necessary and sufficient optimality conditions for (21). The main difficulty compared to finite dimensional barrier methods is that one cannot a-priori exclude that the minimizer approaches the bound $|\boldsymbol{p}|_2 \le \beta$ on parts of the surface, which complicates the discussion of differentiability of the barrier term. The proof uses techniques introduced in [47], where optimal control problems with pointwise simple bounds on the control

and also the state were discussed. Although the present problem is generally simpler due to the absence of state constraints, the nonlinearity of the constraint $|\boldsymbol{p}|_2 \leq \beta$ requires modifications. We therefore do provide the proof of the following theorem but postpone it to the appendix to streamline the presentation. .

Theorem 12. *The vector field $\boldsymbol{p} \in \boldsymbol{H}(\mathrm{div}; S)$ is the unique solution for (21) if and only if $|\boldsymbol{p}|_2 \leq \beta$ holds a.e. on S and*

$$\left(\mathrm{div}\, \boldsymbol{p} + K^* f,\ \mathrm{div}\, \delta\boldsymbol{p}\right)_{B^{-1}} + \mu \int_S \frac{2\,(\boldsymbol{p},\, \delta\boldsymbol{p})_2}{\beta^2 - |\boldsymbol{p}|_2^2}\, \mathrm{d}s = 0 \tag{23}$$

for all $\delta\boldsymbol{p} \in \boldsymbol{H}(\mathrm{div}; S)$.

4.2. Implementation. All numerical studies are based on two different geometries obtained by scanning physical objects with the Artec Eva 3D scanner. The scanner software provides Wavefront .obj files, which contain a description of the geometry via vertices and triangles. In both examples the surface of the scanned object is closed, i.e., without boundary, in accordance with our analysis. The surface texture is provided by the scanner software as a 2D flat bitmap file (see Figure 1, left), together with a mapping of each physical surface triangle into said bitmap. Thus, originally the textured object is described by a varying number of pixels glued onto each surface triangle. Due to the impossibility of continuously mapping a closed surface onto the flat bitmap, there are necessarily discontinuities in the bitmap and there may also be regions which do not appear on the physical surface. Essentially, two adjacent triangles on the surface can be part of discontinuous regions in the texture file. This data is shown in Figure 1 for our first test case.

In order to apply our novel solution scheme, the above mentioned Wavefront object including the texture needs to be made available to the finite element library which is used to discretize the predual barrier problems (21). One way of achieving this is to provide the texture data f at each quadrature point. However, for ease of implementation and processing within the finite element framework FEniCS [36], we instead converted the textured object into the finite element setting by interpolation. To account for both natural discontinuities in the texture as well as the discontinuity of the surface-to-texture mapping, we chose a discontinuous Lagrange (DG) finite element representation of the texture data f. To be more precise, let $\mathcal{P}_r$ define the space of polynomials of maximum degree r, then the texture f and the final output u of our scheme are to fulfill $f_{|K}, u_{|K} \in \mathcal{P}_r$ for all triangles K of the scanned surface. Thus, u and f are elements of the $\mathcal{DG}_r$ finite element space on the surface. The image data f is always scaled to the interval $[0, 1]$.

To carry out the texture preprocessing, we compute the spatial location for each degree of freedom of the surface DG function f within the texture bitmap and use the respective gray value at the nearest pixel. For color textures, this is realized via a vector valued DG function on the surfaces with values in the RGB color space. In the original Wavefront object each surface triangle usually obtains data from multiple texture pixels. Thus, in order to maintain an appropriate quality of the texture in the DG setting, higher order finite element spaces are needed, depending on the quality of the scan. Although in the original Wavefront object the

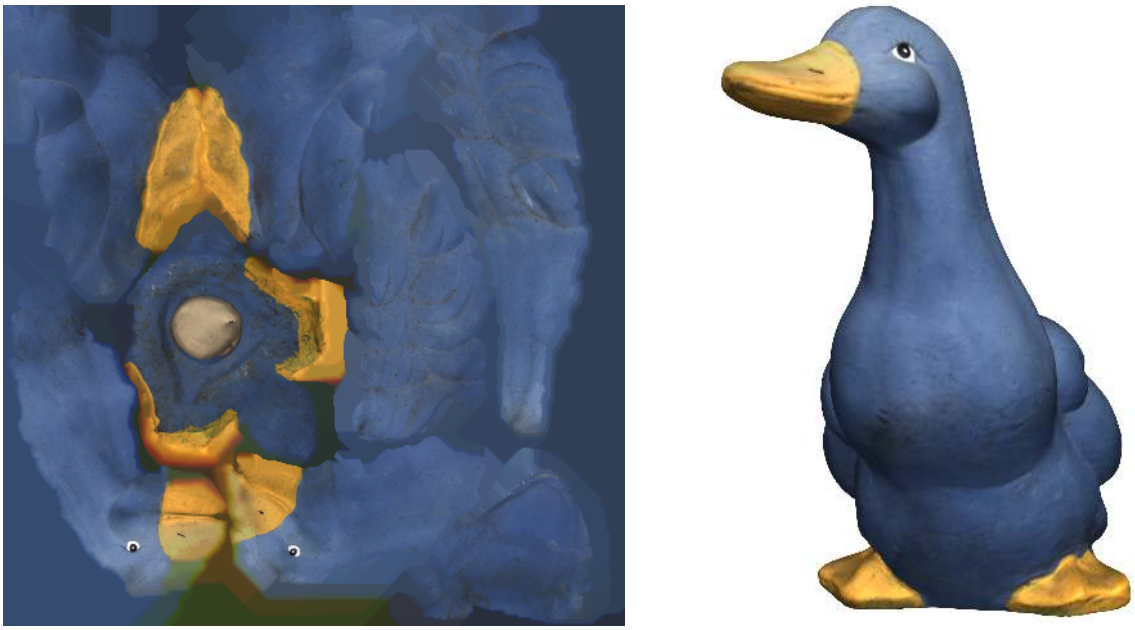

Figure 1. *Left: Texture Bitmap as delivered by the scanner software. Right: Texture mapped onto the geometry.*

number of pixels per triangle may vary significantly, we use a constant finite element order $r = 2$ or $r = 3$ in our examples.

Before recovering the image u we determine the predual (edge detector) vector field $\boldsymbol{p} \in \boldsymbol{H}(\mathrm{div}; S)$ via a sequence of barrier problems (21). For the latter we employ a conforming discretization by surface Raviart–Thomas finite elements. The Raviart–Thomas element space $\mathcal{RT}_{r+1}$ is designed to be the smallest polynomial space with $\mathcal{RT}_{r+1|K} \subset \mathcal{P}_{r+1}$ such that the divergence maps onto $\mathcal{P}_r$; see [43], [27, Chapter 1.4.7] or [36, Ch. 3.4.1]. For our problem the $\mathcal{RT}_{r+1}$ space for the unknown $\boldsymbol{p}$ on the surface is created via mapping the surface element to a flat 2D reference element, as described in [44] and similarly in [35] for the case of linear continuous Lagrange elements. As seen in Theorem 10 we have the relation

$$u = B^{-1}(\mathrm{div}\, \boldsymbol{p} + K^* f). \tag{24}$$

In our examples, which demonstrate denoising and inpainting, K, K^* and therefore B are all pointwise operations which do not involve differentiation. We therefore choose matching polynomial degrees, i.e., $u \in \mathcal{DG}_r$, $\boldsymbol{p} \in \mathcal{RT}_{r+1}$ and $f \in \mathcal{DG}_r$. In terms of finite element functions, (24) is realized by solving an orthogonal projection problem in $L^2(S)$, which is represented by a block-diagonal mass matrix in $\mathcal{DG}_r$ and therefore inexpensive to solve.

5. Numerical Results.

5.1. Gray-Scale Denoising. In this section we consider the classical denoising problem with $K = \mathrm{id}$. The initial test case is the scanned terracotta duck from Figure 1 but with

the texture data converted to a gray scale. Recall that our image data is scaled to a range $[0, 1]$. The geometry consists of $354,330$ triangles and $177,167$ vertices. The surface texture is

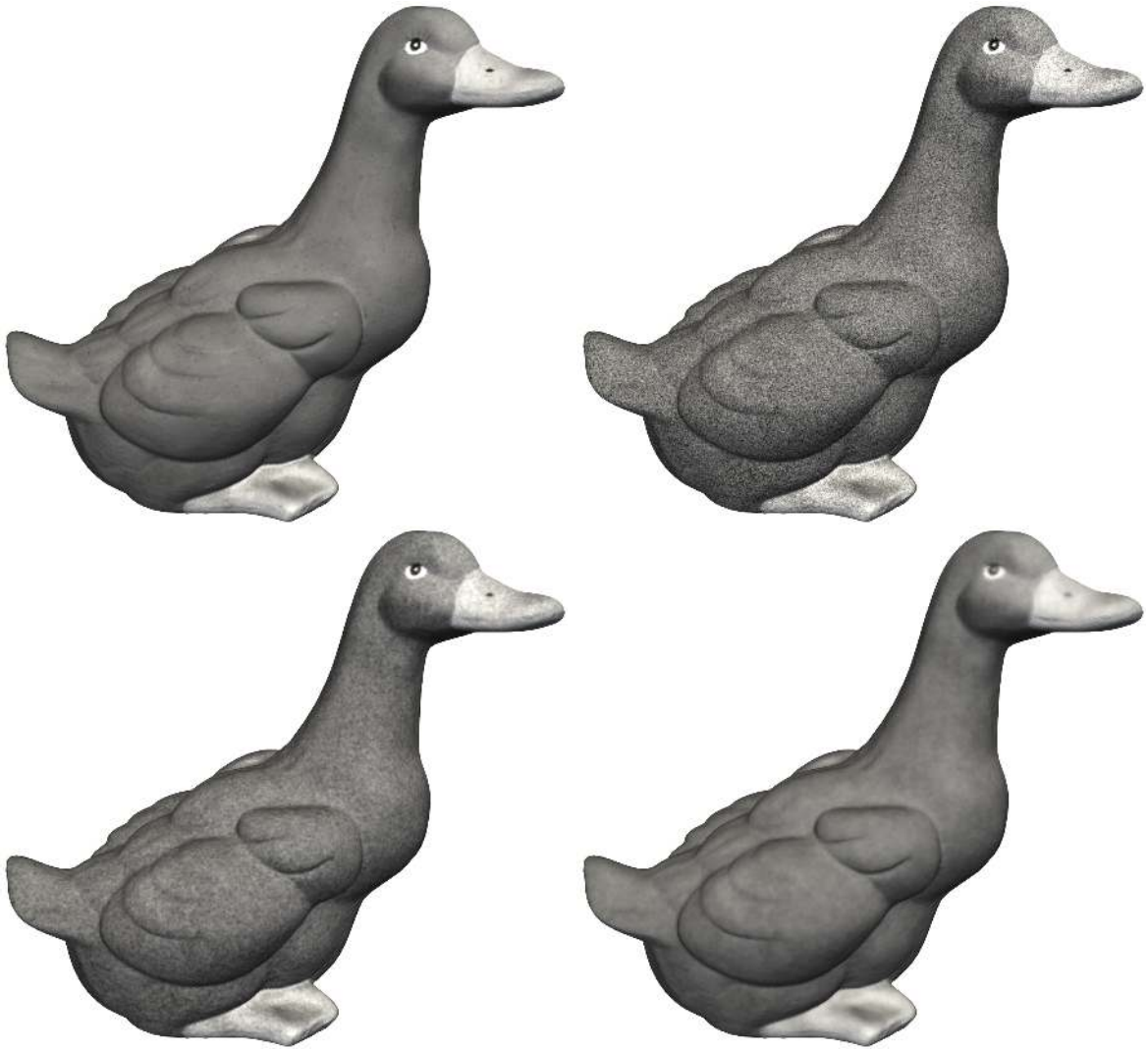

Figure 2. *Duck test case: noise free and noisy originals (top row) and denoising results for* $\beta = 0.1$ *and* $\beta = 0.3$ *(bottom row). The object was kindly scanned by the Rechenzentrum of Würzburg University.*

mostly uniform, however there are some details around the eye and a second order DG function ($r = 2$) manages to resolve these quite well. Also there are sharp interfaces between body, beak and feet. As such, this object provides an excellent first test case and we expect that these interfaces are preserved by the total variation approach.

For simplicity add artificial noise based on a normal distribution with standard deviation $\sigma = 0.1$ and mean value $\mu = 0.0$ to each entry in the coefficient vector representing the image data f. The denoising results shown in Figure 2 were obtained by the interior point method starting from a penalty parameter of $\mu = 1.0$ and stopping at $\mu = 0.02$. For this and the

subsequent color denoising problem described in the following subsection, the value $\alpha = 0.0$ is used and we consider only changes in β. Notice that B in (13) is boundedly invertible even for $\alpha = 0$ since $K = \mathrm{id}$ holds.

For both $\beta = 0.1$ and $\beta = 0.3$ the terminal value for μ was reached after 4 reductions, necessitating the solution of five instances of problem (21) with a Newton scheme. As shown in Figure 3 this did not require more than 5 Newton steps for any value of μ. Total wall-clock time on four non-hyper threaded cores of an Intel i5-4690 CPU running at 3.50 Ghz was slightly less than 40 minutes. Comparing the results shown in Figure 2 one can see that—as expected—with increasing values of β, the noise is reduced more effectively and although the object looks progressively smoother due to a reduction in contrast, sharp corners are preserved. The convergence plots for different values of β are also shown in Figure 3. It is worth noting that the decrease rate of μ in our solver is adaptively based on backtracking, which can be seen in the increasing reduction of μ in the data sets in Figure 3.

5.2. Color Denoising. The second test case consists of a scanned shoe, whose data is provided by the Artec Group Inc.[2] under the Creative Commons Attribution 3.0 Unported License. The shoe consists of exactly $100,000$ triangles and $50,002$ vertices. It provides an excellent second test case because of discontinuous color changes given by the stripes, while at the same time there are also very fine features on the sole and a leathery texture on the outside. Noise is added in the same way to each of the RGB channels as described for the gray-scale test case above. In this example we chose to represent the color texture in terms of a vector valued discontinuous Galerkin function of order $r = 3$. This amounts to problems with 1.8 million degrees of freedom for the predual variable $\boldsymbol{p}$ associated with a single color channel.

The denoising procedure was conducted individually per RGB channel. Initial, noisy and denoised objects are shown in Figure 4. The sharp edges between the stripes are preserved for different values of β. Details of the leather's structure, most prominently visible in the yellow stripes in the noise-free image, start reappearing after the bulk of the noise is removed for $\beta = 0.5$. Notice however that some of these features are part of the geometric resolution and not just the texture. On the other hand, the dotted texture in the interior and part of the stitchings seem less discernible due to the reduced contrast for $\beta = 0.5$. As was noted earlier, the predual vector field $\boldsymbol{p}$ can be interpreted as an edge detector, which is shown in Figure 5 for each RGB channel.

We also conducted experiments using the *joint* BV-norm, cf. [10]

$$\int_S |\nabla \boldsymbol{u}| = \sup \left\{ \int_S \sum_{j=1}^{3} u^j \operatorname{div} \boldsymbol{\eta}^j \, \mathrm{d}s : \boldsymbol{\eta} \in \boldsymbol{W} \right\}$$

of the vector-valued unknown $\boldsymbol{u} = (u^1, u^2, u^3) \in [BV(S)]^3$. In contrast to the scalar case the

[2] https://www.artec3d.com

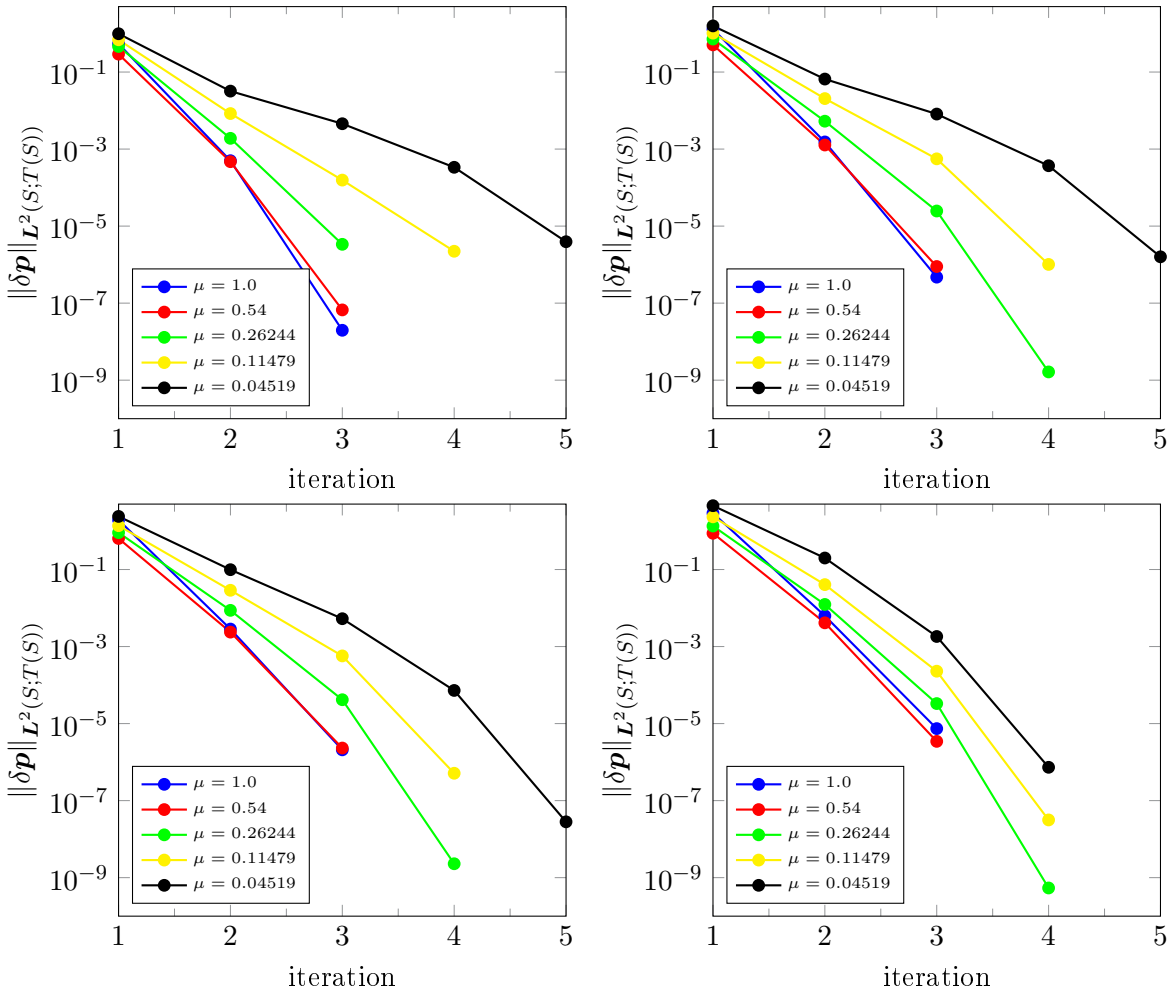

Figure 3. *Convergence of the inner and outer iterations of the interior point method for the duck denoising. Different colors denote outer iterations and their decreasing penalty parameter μ with a stopping criterion of $\|\delta \boldsymbol{p}\|_{\boldsymbol{L}^2(S;T(S))} = 10^{-5}$. Different subplots for respective denoising parameters $\beta = 0.1, 0.2, 0.3, 0.5$.*

test space is now defined as

$$\boldsymbol{W} := \left\{ (\boldsymbol{\eta}^1, \boldsymbol{\eta}^2, \boldsymbol{\eta}^3) \in [\boldsymbol{C}^\infty(S; T(S))]^3 : \sum_{j=1}^{3} |\boldsymbol{\eta}^j(p)|_2^2 \leq 1 \text{ for all } p \in S \right\},$$

compare [12, 24]. It can be expected that this modification better suppresses color fringes (similar to chromatic aberration), which occur when the value of two or more color channels have jump discontinuities at neighboring pixels. We refer the reader to [11, Chapter 6.3.4] for a discussion of alternative definitions of vector-valued BV norms in the context of color image restoration.

Use of the joint BV norm leads to the following modified predual problem compared to

Figure 4. *Shoe test case: noise free and noisy originals (top row) and denoising results for* $\beta = 0.2$ *and* $\beta = 0.5$ *(bottom row).*

Figure 5. *Shoe test case:* $|\boldsymbol{p}|_2$ *acts as an edge detector for each RGB channel. Solid black corresponds to a value of* $|\boldsymbol{p}|_2 \geq 0.4$. *Final results for* $\beta = 0.5$ *are shown. Take note of the different jump amplitudes and positions for each color channel.*

(14),

$$\begin{cases} \text{Minimize} & \dfrac{1}{2}\left\| \begin{pmatrix} \operatorname{div} \boldsymbol{p}^1 \\ \operatorname{div} \boldsymbol{p}^2 \\ \operatorname{div} \boldsymbol{p}^3 \end{pmatrix} + K^* \boldsymbol{f} \right\|_{B^{-1}}^2 \\ \text{over} & (\boldsymbol{p}^1, \boldsymbol{p}^2, \boldsymbol{p}^3) \in [\boldsymbol{H}(\operatorname{div}; S)]^3 \\ \text{subject to} & \displaystyle\sum_{j=1}^{3} |\boldsymbol{p}^j|_2^2 \leq \beta^2 \quad \text{a.e. on } S, \end{cases}$$

see also [12]. Notice that the variables $\boldsymbol{p}^j$ in this problem are *coupled* through the inequality constraints even if — as is the case in our examples — K and K^* act on each color component separately. This leads to an increased complexity of the problem. The conversion of the inequality constraints into a barrier term as in (21) is straightforward. In our numerical experiments, we did not experience significantly improved results using this model and therefore do not pursue this further here.

5.3. Color Inpainting. The problem of not being able to scan an object completely is quite common, as there might be areas the scanner cannot look into due to its size and the non-convexity and curvature of the object. The inside of the tip of a shoe might be such an example. Data corruption can be another reason for lack or loss of data. Although these issue concern both geometry and texture, the focus of this subsection is on the reconstruction of missing texture information alone.

We simulate the loss of texture data during the scan process on the *outside* of an object by setting to zero all degrees of freedom in the image data which belong to cells with indices in the range $30,000$ to $33,000$. This corresponds to a data loss of 3%. We denote this

erased image region by $E \subset S$. Due to the apparently layered scan process the index range chosen corresponds to bands or "stripes" as shown in Figure 6, which are better visible than unreachable areas inside the tip.

Figure 6. *Shoe with missing texture (top left) and TV-inpainting solutions for* $\beta = 0.5$, $\beta = 0.7$ *and* $\beta = 1.0$.

As usual for TV inpainting problems the mapping K is now chosen so as to ignore the corrupted data. This leads to

$$(Ku)(p) := \chi_{S\setminus E}(p)\, u(p), \tag{25}$$

where χ is an indicator function with value 1 in the uncorrupted area $S \setminus E$. Since K is

self-adjoint and idempotent,

$$K^*(Ku) = K(Ku) = Ku.$$

$(Ku)(p) - f(p) = 0$ holds for all $p \in E$ and the (corrupted) value of $f_{|E}$ does not increase the data fidelity part of the objective in (1).

Contrary to the denoising situation, K^*K is no longer invertible and $\alpha > 0$ is required. Using the definition of K one easily deduces the formula

$$(B\,u)(p) = \begin{cases} \alpha\, u(p) & \text{for } p \in E \\ (\alpha + 1)\, u(p) & \text{for } p \in S \setminus E. \end{cases}$$

The results of the inpainting test case are shown in Figure 6 for different values of β and with $\alpha = 0.1$ constant for each case.

6. Conclusion and Outlook. We considered an analog of the TV–L^2 image reconstruction approach for images on smooth surfaces. Complementary to [35], we proved the well-posedness of the model and its predual, and rigorously established strong duality with the predual in function space. The predual problem is a quadratic optimization problem for the vector field $\boldsymbol{p} \in \boldsymbol{H}(\mathrm{div}; S)$ with pointwise nonlinear inequality constraints on the surface. As in the flat case, $\boldsymbol{p}$ serves as an edge detector. We proposed and analyzed a function space interior point method for the predual problem. Based on the finding that the latter is posed in $\boldsymbol{H}(\mathrm{div}; S)$, we are led to choose a conforming finite element discretization by the surface analog of first- or higher-order Raviart–Thomas finite element spaces. In contrast to linear Lagrangian elements employed in [35], our discretization exhausts the space when the surface mesh is refined. Numerical examples, which comprise denoising and inpainting problems, show the viability of the approach for real-world geometries consisting of more than $350,000$ and $175,000$ vertices. Our method can be easily adapted to surfaces with boundary, by replacing $\boldsymbol{H}(\mathrm{div}; S)$ with $\boldsymbol{H}_0(\mathrm{div}; S)$. This amounts to imposing the boundary condition $\boldsymbol{p} \cdot \boldsymbol{n} = 0$ along the boundary ∂S, where $\boldsymbol{n}$ is the outer unit normal vector in the tangent plane. The analysis presented carries over with minor changes.

There is room for improvement in various directions. For instance, the polynomial order r of the finite element space $\mathcal{DG}_r$ for the image data f could be adjusted locally to reflect the level of detail present in each surface cell. This would then naturally lead to discretizations of $\boldsymbol{p}$ and u with varying polynomial degree as well. Moreover, we have so far been solving the predual problem with a basic primal interior point approach, running Newton's method to convergence for each value of the barrier parameter μ. A more sophisticated primal-dual method with inexact system solves would help reduce the computational cost for high-dimensional problems. While we are exploiting the MPI-based parallelism of the FEniCS library for system assembly and direct system solves already, more efficiency might be gained by preconditioned iterative solvers with tailored preconditioners. This is left for future research.

Appendix A. Proof of Theorem 12 and Auxiliary Results. Let us denote by

$$\ell(\boldsymbol{p}) := \begin{Bmatrix} -\mu \ln\left(\beta^2 - |\boldsymbol{p}|_2^2\right) & \text{if } |\boldsymbol{p}|_2 < \beta \\ \infty & \text{otherwise} \end{Bmatrix} \quad \text{and} \quad \nabla\ell(\boldsymbol{p}) = 2\,\mu\,\frac{\boldsymbol{p}}{\beta^2 - |\boldsymbol{p}|_2^2} \quad \text{if } |\boldsymbol{p}|_2 < \beta$$

the pointwise barrier term and its gradient[3], defined for $\boldsymbol{p} \in \mathbb{R}^3$ and in particular for $\boldsymbol{p}$ in the tangent space $T_p(S)$ of the surface S at some point. Moreover, let

$$b(\boldsymbol{p}) := \int_S \ell(\boldsymbol{p})\,\mathrm{d}s \quad \text{and} \quad \langle b'(\boldsymbol{p}),\, \delta\boldsymbol{p}\rangle := \int_S \left(\nabla\ell(\boldsymbol{p}),\, \delta\boldsymbol{p}\right)_2 \mathrm{d}s$$

denote the integrated barrier term (cf. (22)) and its *formal* derivative for vector fields $\boldsymbol{p}, \delta\boldsymbol{p} \in \boldsymbol{L}^2(S;T(S))$. Let us recall from the proof of Proposition 11 that b is convex and it can take values in $\mathbb{R} \cup \{\infty\}$. We denote by $\partial b(\boldsymbol{p}) \subset \boldsymbol{L}^2(S;T(S))^*$ the convex subdifferential of b at $\boldsymbol{p}$. Notice that $\boldsymbol{L}^2(S;T(S))^*$ can be identified with $\boldsymbol{L}^2(S;T(S)^*)$ and also with $\boldsymbol{L}^2(S;T(S))$.

Before stating the proof of Theorem 12 we require some preliminary results. The following lemma parallels [47, Lemma 4.4] and its proof is therefore omitted.

Lemma 13. *Consider $\boldsymbol{p}, \delta\boldsymbol{p} \in \boldsymbol{L}^2(S;T(S))$ such that all of $b(\boldsymbol{p})$, $b(\boldsymbol{p}+\delta\boldsymbol{p})$ and $\langle b'(\boldsymbol{p}),\, \delta\boldsymbol{p}\rangle$ are finite. Then b is directionally differentiable at $\boldsymbol{p}$ in the direction $\delta\boldsymbol{p}$, and its directional derivative satisfies*

$$b'(\boldsymbol{p};\delta\boldsymbol{p}) = \langle b'(\boldsymbol{p}),\, \delta\boldsymbol{p}\rangle \geq \int_S (\boldsymbol{m},\, \delta\boldsymbol{p})_2\,\mathrm{d}s \quad \textit{for all } \boldsymbol{m} \in \partial b(\boldsymbol{p}), \tag{26}$$

where the subdifferential is considered a subset of $\boldsymbol{L}^2(S;T(S))$.

The next result is equal to [47, Prop. 4.5] but the proof requires a number of modifications.

Proposition 14. *Let $\boldsymbol{p} \in \boldsymbol{L}^2(S;T(S))$ be given. Then we have:*

(*i*) *If $\nabla\ell(\boldsymbol{p})$ belongs to $\boldsymbol{L}^2(S;T(S))$, then $\partial b(\boldsymbol{p}) = \{\nabla\ell(\boldsymbol{p})\}$.*

(*ii*) *If $\nabla\ell(\boldsymbol{p})$ does not belong to $\boldsymbol{L}^2(S;T(S))$, then $\partial b(\boldsymbol{p}) = \emptyset$.*

Proof. The proof is split into three parts, which combine to yield the result.

Part A: We begin by considering the case $b(\boldsymbol{p}) < \infty$, which implies $|\boldsymbol{p}|_2 < \beta$ a.e. on S. By convexity of ℓ, we obtain $(\nabla\ell(\boldsymbol{p}),\, \delta\boldsymbol{p})_2 \leq \ell(\boldsymbol{p}+\delta\boldsymbol{p}) - \ell(\boldsymbol{p})$ a.e. and therefore

$$\int_S \left(\nabla\ell(\boldsymbol{p}),\, \delta\boldsymbol{p}\right)_2 \mathrm{d}s = \langle b'(\boldsymbol{p}),\, \delta\boldsymbol{p}\rangle \leq b(\boldsymbol{p}+\delta\boldsymbol{p}) - b(\boldsymbol{p})$$

for all $\delta\boldsymbol{p} \in \boldsymbol{L}^2(S;T(S))$, provided that $\nabla\ell(\boldsymbol{p}) \in \boldsymbol{L}^2(S;T(S))$ holds. This shows $\nabla\ell(\boldsymbol{p}) \in \partial b(\boldsymbol{p})$ in this case.

[3]This should not be confused with the gradient of a scalar function on S in Definition 4. In the present context the *gradient* $\nabla\ell(\boldsymbol{p})$ is the transpose of the derivative of the function $\ell : \mathbb{R}^3 \to \mathbb{R}$.

Part B: Now suppose that $\boldsymbol{m} \in \partial b(\boldsymbol{p})$ holds and let $E \subset S$ be an arbitrary measurable subset and $\boldsymbol{v} : S \to T(S)$ be a vector field of class C^0. Due to the compactness of S, $\|\boldsymbol{v}\|_{\boldsymbol{L}^\infty(S;T(S))}$ is finite. We are going to show that necessarily

$$(*) \qquad \int_E \big(\nabla \ell(\boldsymbol{p}),\, \boldsymbol{v}\big)_2 \,\mathrm{d}s = \int_E (\boldsymbol{m},\, \boldsymbol{v})_2 \,\mathrm{d}s$$

holds, which then implies $\boldsymbol{m} = \nabla \ell(\boldsymbol{p})$ and $\nabla \ell(\boldsymbol{p}) \in \boldsymbol{L}^2(S;T(S))$. To this end, define $E_\delta := \{p \in E : \beta - |\boldsymbol{p}|_2 > \delta\}$ for $\delta > 0$. Next we define $\boldsymbol{v}_k := \chi_{E_{1/k}} \boldsymbol{v}$ and $\varepsilon_k := (2\,k\,\|\boldsymbol{v}\|_{\boldsymbol{L}^\infty(S;T(S))})^{-1}$ for $k \in \mathbb{N}$. Then, since $\nabla \ell(\boldsymbol{p}) = 2\,\mu\,\frac{\boldsymbol{p}}{\beta^2 - |\boldsymbol{p}|_2^2}$ belongs to $\boldsymbol{L}^\infty(E_\delta;T(S))$ for any $\delta > 0$, we have

$$\big|\langle b'(\boldsymbol{p}),\, \pm\varepsilon_k \boldsymbol{v}_k\rangle\big| = \pm 2\,\mu\,\varepsilon_k \int_{E_{1/k}} \frac{(\boldsymbol{p},\, \boldsymbol{v}_k)_2}{\beta^2 - |\boldsymbol{p}|_2^2} \,\mathrm{d}s < \infty.$$

Moreover,

$$(**) \qquad b(\boldsymbol{p} \pm \varepsilon_k \boldsymbol{v}_k) = -\mu \int_{S \setminus E_{1/k}} \ln\big(\beta^2 - |\boldsymbol{p}|_2^2\big) \,\mathrm{d}s - \mu \int_{E_{1/k}} \ln\big(\beta^2 - |\boldsymbol{p} \pm \varepsilon_k \boldsymbol{v}_k|_2^2\big) \,\mathrm{d}s.$$

The first integral is finite since $b(\boldsymbol{p})$ is. For the second integral, we use that

$$\beta - |\boldsymbol{p} \pm \varepsilon_k \boldsymbol{v}_k|_2 \geq \beta - |\boldsymbol{p}|_2 - \varepsilon_k \|\boldsymbol{v}\|_{\boldsymbol{L}^\infty(S;T(S))} \geq \frac{1}{k} - \frac{1}{2\,k} = \frac{1}{2\,k}$$

holds a.e. on $E_{1/k}$. Hence by multiplication with $\beta + |\boldsymbol{p} \pm \varepsilon_k \boldsymbol{v}_k|_2 \geq \beta$ we conclude

$$\beta^2 - |\boldsymbol{p} \pm \varepsilon_k \boldsymbol{v}_k|_2^2 \geq \frac{\beta}{2\,k} \quad \text{a.e. on } E_{1/k}$$

and thus the second integral in $(**)$ is finite as well. So we have shown that for $\delta\boldsymbol{p} = \pm\varepsilon_k \boldsymbol{v}_k$, the terms $b(\boldsymbol{p})$, $b(\boldsymbol{p} + \delta\boldsymbol{p})$ and $\langle b'(\boldsymbol{p}),\, \delta\boldsymbol{p}\rangle$ are all finite. Hence Lemma 13 yields

$$\langle b'(\boldsymbol{p}),\, \pm\varepsilon_k \boldsymbol{v}_k\rangle \geq \pm\varepsilon_k \int_S (\boldsymbol{m},\, \boldsymbol{v}_k)_2 \,\mathrm{d}s \quad \text{for all } \boldsymbol{m} \in \partial b(\boldsymbol{p}).$$

This implies

$$(***) \qquad \int_S \big(\nabla \ell(\boldsymbol{p}),\, \boldsymbol{v}_k\big)_2 \,\mathrm{d}s = \langle b'(\boldsymbol{p}),\, \boldsymbol{v}_k\rangle = \int_S (\boldsymbol{m},\, \boldsymbol{v}_k)_2 \,\mathrm{d}s \quad \text{for all } \boldsymbol{m} \in \partial b(\boldsymbol{p}), k \in \mathbb{N}.$$

It remains to pass to the limit in $(***)$ to show $(*)$. Let us begin with the second term in $(***)$ and observe that $\chi_E\, \boldsymbol{v} = \lim_{k\to\infty} \boldsymbol{v}_k$ holds a.e. on S since the set where $|\boldsymbol{p}|_2 = \beta$ holds has zero measure. Moreover, the integrand is dominated pointwise by $|(\boldsymbol{m},\, \boldsymbol{v}_k)_2| \leq |\boldsymbol{m}|_2 \|\boldsymbol{v}\|_{\boldsymbol{L}^\infty(S;T(S))} \in L^2(S)$. Thus by Lebesgue's dominated convergence theorem we obtain

$$\lim_{k\to\infty} \int_S (\boldsymbol{m},\, \boldsymbol{v}_k)_2 \,\mathrm{d}s = \int_E (\boldsymbol{m},\, \boldsymbol{v})_2 \,\mathrm{d}s.$$

We now address the first term in $(***)$. Since it is not clear whether or not $\nabla\ell(\boldsymbol{p})$ belongs to $\boldsymbol{L}^2(S;T(S))$, we cannot argue by dominated convergence. Instead, let us define

$$S^+ := \{p \in S : (\boldsymbol{p}, \boldsymbol{v})_2 \geq 0\} \quad \text{and} \quad S^- := S \setminus S^+.$$

Then

$$\chi_{S^+}\big(\nabla\ell(\boldsymbol{p}), \boldsymbol{v}_k\big)_2 = \begin{cases} 2\,\mu\,\frac{(\boldsymbol{p},\boldsymbol{v})_2}{\beta^2 - |\boldsymbol{p}|_2^2} \geq 0 & \text{on } S^+ \cap E_{1/k} \\ 0 & \text{elsewhere} \end{cases}$$

and therefore $\{\chi_{S^+}\big(\nabla\ell(\boldsymbol{p}), \boldsymbol{v}_k\big)_2\}_{k\in\mathbb{N}}$ is non-negative and monotone increasing on S^+ with pointwise limit $\chi_{S^+\cap E}\big(\nabla\ell(\boldsymbol{p}), \boldsymbol{v}\big)_2$. By the monotone convergence theorem,

$$\lim_{k\to\infty} \int_{S^+} \big(\nabla\ell(\boldsymbol{p}), \boldsymbol{v}_k\big)_2 \,\mathrm{d}s = \int_{S^+\cap E} \big(\nabla\ell(\boldsymbol{p}), \boldsymbol{v}\big)_2 \,\mathrm{d}s$$

holds. Similarly, this result can be shown with S^- as well. We can therefore pass to the limit in $(***)$ and conclude $(*)$, which in turn proves $\boldsymbol{m} = \nabla\ell(\boldsymbol{p})$ as well as $\nabla\ell(\boldsymbol{p}) \in \boldsymbol{L}^2(S;T(S))$.

Part C: If $b(\boldsymbol{p}) = \infty$, then by definition $\partial b(\boldsymbol{p}) = \emptyset$ holds.

The result now follows easily by combining Parts A–C. ∎

So far we have considered the subdifferential of the barrier term b w.r.t. the $\boldsymbol{L}^2(S;T(S))$ topology. This is however not sufficient since problem (21) is posed in $\boldsymbol{H}(\mathrm{div};S)$ and further modifications of the arguments in [47] are required. Let us define by $\widetilde{b}$ the restriction of b to $\boldsymbol{H}(\mathrm{div};S)$, and let

$$\partial\widetilde{b}(\boldsymbol{p}) := \Big\{\widetilde{\boldsymbol{m}} \in \boldsymbol{H}(\mathrm{div};S) : \widetilde{b}(\boldsymbol{q}) \geq \widetilde{b}(\boldsymbol{p}) + (\widetilde{\boldsymbol{m}}, \boldsymbol{q}-\boldsymbol{p})_{\boldsymbol{H}(\mathrm{div};S)} \quad \text{for all } \boldsymbol{q} \in \boldsymbol{H}(\mathrm{div};S)\Big\} \tag{27}$$

denote the subdifferential of $\widetilde{b}$ at $\boldsymbol{p} \in \boldsymbol{H}(\mathrm{div};S)$. Finally, $\Pi : \boldsymbol{L}^2(S;T(S)) \to \boldsymbol{H}(\mathrm{div};S)$ denotes the $\boldsymbol{H}(\mathrm{div};S)$-orthogonal projector, defined by

$$\widetilde{\boldsymbol{m}} = \Pi\,\boldsymbol{m} \quad \Leftrightarrow \quad (\widetilde{\boldsymbol{m}}, \boldsymbol{z})_{\boldsymbol{H}(\mathrm{div};S)} = (\boldsymbol{m}, \boldsymbol{z})_{\boldsymbol{L}^2(S;T(S))} \quad \text{for all } \boldsymbol{z} \in \boldsymbol{H}(\mathrm{div};S).$$

Corollary 15. *Let $\boldsymbol{p} \in \boldsymbol{H}(\mathrm{div};S)$ be given. Then we have $\partial\widetilde{b}(\boldsymbol{p}) = \Pi\,\partial b(\boldsymbol{p})$ and consequently:*

(*i*) *If $\nabla\ell(\boldsymbol{p})$ belongs to $\boldsymbol{L}^2(S;T(S))$, then $\partial\widetilde{b}(\boldsymbol{p}) = \{\Pi\,\nabla\ell(\boldsymbol{p})\}$.*

(*ii*) *If $\nabla\ell(\boldsymbol{p})$ does not belong to $\boldsymbol{L}^2(S;T(S))$, then $\partial\widetilde{b}(\boldsymbol{p}) = \emptyset$.*

Proof. Let $\Lambda : \boldsymbol{H}(\mathrm{div};S) \to \boldsymbol{L}^2(S;T(S))$ denote the continuous embedding, and let $\Lambda^* : \boldsymbol{L}^2(S;T(S))^* \to \boldsymbol{H}(\mathrm{div};S)^*$ denote its adjoint. Since by definition $\widetilde{b}(\boldsymbol{p}) = b(\Lambda\boldsymbol{p})$ and $\Lambda\boldsymbol{p} = \boldsymbol{p}$ holds for all $\boldsymbol{p} \in \boldsymbol{H}(\mathrm{div};S)$, we conclude from the chain rule that

$$\mathcal{R}_{\boldsymbol{H}(\mathrm{div};S)}\partial\widetilde{b}(\boldsymbol{p}) = \Lambda^*\mathcal{R}_{\boldsymbol{L}^2(S;T(S))}\partial b(\Lambda\boldsymbol{p}) = \Lambda^*\mathcal{R}_{\boldsymbol{L}^2(S;T(S))}\partial b(\boldsymbol{p})$$

holds; see for instance [25, Prop. I.5.7]. Notice that the Riesz maps $\mathcal{R}_{\boldsymbol{H}(\mathrm{div};S)} : \boldsymbol{H}(\mathrm{div};S) \to \boldsymbol{H}(\mathrm{div};S)^*$ and $\mathcal{R}_{\boldsymbol{L}^2(S;T(S))} : \boldsymbol{L}^2(S;T(S)) \to \boldsymbol{L}^2(S;T(S))^*$ are present here since we identify the subdifferential in both Hilbert spaces with elements from the Hilbert space itself; cf. (27). We have thus shown that

$$\partial\widetilde{b}(\boldsymbol{p}) = \mathcal{R}^{-1}_{\boldsymbol{H}(\mathrm{div};S)}\Lambda^*\mathcal{R}_{\boldsymbol{L}^2(S;T(S))}\partial b(\boldsymbol{p})$$

holds for all $\boldsymbol{p} \in \boldsymbol{H}(\mathrm{div};S)$. It is now an easy exercise to verify that $\mathcal{R}^{-1}_{\boldsymbol{H}(\mathrm{div};S)}\Lambda^*\mathcal{R}_{\boldsymbol{L}^2(S;T(S))}$ is equal to Π. ∎

Proof of Theorem 12. Recall from (22) the definition of H and b and let us denote, as above, by $\widetilde{b}$ the restriction of b to $\boldsymbol{H}(\mathrm{div};S)$. The (unique) minimizer of (21) is characterized by

$$0 \in \partial\big(H(\boldsymbol{p}) + \widetilde{b}(\boldsymbol{p})\big).$$

Since H is continuous on all of $\boldsymbol{H}(\mathrm{div};S)$ and $\widetilde{b}$ is finite e.g., at $\boldsymbol{p} \equiv \boldsymbol{0}$, this is equivalent to

$$0 \in \partial H(\boldsymbol{p}) + \partial\widetilde{b}(\boldsymbol{p})$$

by the sum rule of subdifferentials; see for instance [25, Prop. I.5.6]. Notice that this also implies $|\boldsymbol{p}|_2 \le \beta$ a.e. on S since otherwise $\widetilde{b}(\boldsymbol{p}) = \infty$ and the subdifferential is empty. Having characterized $\partial\widetilde{b}(\boldsymbol{p})$ in Corollary 15 and using the obvious Fréchet differentiability of H, we can write equivalently (using the notation from Corollary 15)

$$\begin{aligned}
& 0 = \mathcal{R}^{-1}_{\boldsymbol{H}(\mathrm{div};S)}H'(\boldsymbol{p}) + \Pi\,\nabla\ell(\boldsymbol{p}) \\
\Leftrightarrow\quad & 0 = \mathcal{R}^{-1}_{\boldsymbol{H}(\mathrm{div};S)}H'(\boldsymbol{p}) + \mathcal{R}^{-1}_{\boldsymbol{H}(\mathrm{div};S)}\Lambda^*\mathcal{R}_{\boldsymbol{L}^2(S;T(S))}\nabla\ell(\boldsymbol{p}) \\
\Leftrightarrow\quad & 0 = H'(\boldsymbol{p})\,\delta\boldsymbol{p} + \langle\Lambda^*\mathcal{R}_{\boldsymbol{L}^2(S;T(S))}\nabla\ell(\boldsymbol{p}),\,\delta\boldsymbol{p}\rangle_{\boldsymbol{H}(\mathrm{div};S)^*,\boldsymbol{H}(\mathrm{div};S)} && \text{for all } \delta\boldsymbol{p} \in \boldsymbol{H}(\mathrm{div};S) \\
\Leftrightarrow\quad & 0 = H'(\boldsymbol{p})\,\delta\boldsymbol{p} + \langle\mathcal{R}_{\boldsymbol{L}^2(S;T(S))}\nabla\ell(\boldsymbol{p}),\,\Lambda\delta\boldsymbol{p}\rangle_{\boldsymbol{L}^2(S;T(S))^*,\boldsymbol{L}^2(S;T(S))} && \text{for all } \delta\boldsymbol{p} \in \boldsymbol{H}(\mathrm{div};S) \\
\Leftrightarrow\quad & 0 = H'(\boldsymbol{p})\,\delta\boldsymbol{p} + (\nabla\ell(\boldsymbol{p}),\,\Lambda\delta\boldsymbol{p})_{\boldsymbol{L}^2(S;T(S))} && \text{for all } \delta\boldsymbol{p} \in \boldsymbol{H}(\mathrm{div};S).
\end{aligned}$$

This is precisely (23).

Acknowledgments. Parts of this paper were written while the second author was visiting the University of British Columbia, Vancouver. He would like to thank the Department of Computer Science for their hospitality.

REFERENCES

[1] H. Attouch, G. Buttazzo, and G. Michaille, *Variational analysis in Sobolev and BV spaces*, vol. 6 of MPS/SIAM Series on Optimization, Society for Industrial and Applied Mathematics (SIAM), Philadelphia, PA, 2006.

[2] T. Aubin, *A course in differential geometry*, vol. 27 of Graduate Studies in Mathematics, American Mathematical Society, Providence, RI, 2001.

[3] C. L. Bajaj and G. Xu, *Anisotropic diffusion of surfaces and functions on surfaces*, ACM Transactions on Graphics, 22 (2003), pp. 4–32.

[4] S. Bartels, *Total variation minimization with finite elements: convergence and iterative solution*, SIAM Journal on Numerical Analysis, 50 (2012), pp. 1162–1180, https://doi.org/10.1137/11083277X.

[5] S. Bartels, *Error control and adaptivity for a variational model problem defined on functions of bounded variation*, Mathematics of Computation, 84 (2015), pp. 1217–1240, https://doi.org/10.1090/S0025-5718-2014-02893-7.

[6] M. Ben-Artzi and P. G. LeFloch, *Well-posedness theory for geometry-compatible hyperbolic conservation laws on manifolds*, Annales de l'Institut Henri Poincaré. Analyse Non Linéaire, 24 (2007), pp. 989–1008, https://doi.org/10.1016/j.anihpc.2006.10.004.

[7] H. Benninghoff and H. Garcke, *Segmentation and restoration of images on surfaces by parametric active contours with topology changes*, Journal of Mathematical Imaging and Vision, 55 (2016), pp. 105–124, https://doi.org/10.1007/s10851-015-0616-6.

[8] M. Bertalmío, L.-T. Cheng, S. Osher, and G. Sapiro, *Variational problems and partial differential equations on implicit surfaces*, Journal of Computational Physics, 174 (2001), pp. 759–780, https://doi.org/10.1006/jcph.2001.6937.

[9] H. Biddle, I. von Glehn, C. B. Macdonald, and T. März, *A volume-based method for denoising on curved surfaces*, in 2013 IEEE International Conference on Image Processing, IEEE, sep 2013, pp. 529–533, https://doi.org/10.1109/icip.2013.6738109.

[10] P. Blomgren and T. Chan, *Color TV: total variation methods for restoration of vector-valued images*, IEEE Transactions on Image Processing, 7 (1998), pp. 304–309, https://doi.org/10.1109/83.661180.

[11] K. Bredies and D. Lorenz, *Mathematische Bildverarbeitung*, Vieweg & Teubner, 2011, https://doi.org/10.1007/978-3-8348-9814-2.

[12] X. Bresson and T. F. Chan, *Fast dual minimization of the vectorial total variation norm and applications to color image processing*, Inverse Problems and Imaging, 2 (2008), pp. 455–484, https://doi.org/10.3934/ipi.2008.2.455.

[13] J.-F. Cai, S. Osher, and Z. Shen, *Linearized Bregman iterations for frame-based image deblurring*, SIAM Journal on Imaging Sciences, 2 (2009), pp. 226–252, https://doi.org/10.1137/080733371.

[14] J. L. Carter, *Dual Methods for Total Variation-Based Image Restoration*, PhD thesis, UCLA, 2001.

[15] A. Chambolle, *An algorithm for total variation minimization and applications*, Journal of Mathematical Imaging and Vision, 20 (2004), pp. 89–97, https://doi.org/10.1023/B:JMIV.0000011325.36760.1e. Special issue on mathematics and image analysis.

[16] A. Chambolle and P.-L. Lions, *Image recovery via total variation minimization and related problems*, Numerische Mathematik, 76 (1997), pp. 167–188, https://doi.org/10.1007/s002110050258.

[17] T. Chan, S. Esedoglu, F. Park, and A. Yip, *Total variation image restoration: overview and recent developments*, in Handbook of mathematical models in computer vision, Springer, New York, 2006, pp. 17–31, https://doi.org/10.1007/0-387-28831-7_2.

[18] T. F. Chan, G. H. Golub, and P. Mulet, *A nonlinear primal-dual method for total variation-based image restoration*, SIAM Journal on Scientific Computing, 20 (1999), pp. 1964–1977, https://doi.org/10.1137/S1064827596299767.

[19] T. F. Chan and J. Shen, *Image processing and analysis*, Society for Industrial and Applied Mathematics (SIAM), Philadelphia, PA, 2005, https://doi.org/10.1137/1.9780898717877. Variational, PDE, wavelet, and stochastic methods.

[20] U. Clarenz, U. Diewald, and M. Rumpf, *Processing textured surfaces via anisotropic geometric diffusion*, IEEE Transactions on Image Processing, 13 (2004), pp. 248–261, https://doi.org/10.1109/tip.2003.819863.

[21] M. Desbrun, M. Meyer, P. Schröder, and A. H. Barr, *Anisotropic feature-preserving denoising of height fields and bivariate data*, in Proceedings of Graphics Interface 2000, Toronto, Ontario, Canada, 2000, Canadian Human-Computer Communications Society, pp. 145–152, https://doi.org/10.20380/GI2000.20.

[22] M. P. do Carmo, *Riemannian geometry*, Mathematics: Theory & Applications, Birkhäuser Boston, Inc., Boston, MA, 1992. Translated from the second Portuguese edition by Francis Flaherty.

[23] D. C. Dobson and F. Santosa, *Recovery of blocky images from noisy and blurred data*, SIAM Journal on Applied Mathematics, 56 (1996), pp. 1181–1198, https://doi.org/10.1137/S003613999427560X.

[24] Y. Dong, M. Hintermüller, and M. M. Rincon-Camacho, *A multi-scale vectorial L^τ-TV framework for color image restoration*, International Journal of Computer Vision, 92 (2011), pp. 296–307, https://doi.org/10.1007/s11263-010-0359-1.

[25] I. Ekeland and R. Temam, *Convex Analysis and Variational Problems*, vol. 28 of Classics in Applied Mathematics, SIAM, Philadelphia, 1999.

[26] G. Enrico, *Minimal Surfaces and Functions of Bounded Variation*, vol. 80 of Monographs in Mathematics, Birkäuser, 1984.

[27] A. Ern and J.-L. Guermond, *Theory and Practice of Finite Elements*, Springer, Berlin, 2004.

[28] E. Hebey, *Sobolev Spaces on Riemannian Manifolds*, vol. 1635 of Lecture Notes in Mathematics, Springer, 1996.

[29] E. Hebey, *Nonlinear Analysis on Manifolds*, vol. 5 of American Mathematical Society, Courant Lectures Notes in Mathematics, 2000.

[30] R. Herzog, G. Stadler, and G. Wachsmuth, *Directional sparsity in optimal control of partial differential equations*, SIAM Journal on Control and Optimization, 50 (2012), pp. 943–963, https://doi.org/10.1137/100815037.

[31] M. Hintermüller and K. Kunisch, *Total bounded variation regularization as a bilaterally constrained optimization problem*, SIAM Journal on Applied Mathematics, 64 (2004), pp. 1311–1333, https://doi.org/10.1137/S0036139903422784.

[32] J. R. Jensen, *Introductory Digital Image Processing: A Remote Sensing Perspective*, Prentice-Hall Inc., Englewood Cliffs, N.J., 4th ed., 2015.

[33] J. John and M. Wilscy, *Image processing techniques for surface characterization of nanostructures*, in 2016 International Conference on Circuit, Power and Computing Technologies (ICCPCT), IEEE, mar 2016, https://doi.org/10.1109/iccpct.2016.7530317.

[34] W. Kühnel, *Differentialgeometrie*, vol. 6 of Aufbaukurs Mathematik, Springer Spektrum, 2013.

[35] R. Lai and T. F. Chan, *A framework for intrinsic image processing on surfaces*, Computer Vision and Image Understanding, 115 (2011), pp. 1647–1661, https://doi.org/10.1016/j.cviu.2011.05.011.

[36] A. Logg, K.-A. Mardal, and G. Wells, eds., *Automated Solution of Differential Equations by the Finite Element Method*, vol. 84 of Lecture Notes in Computational Science and Engineering, Springer Berlin Heidelberg, 2012.

[37] L. D. López Pérez, *Régularisation d'images sur des surfaces non planes*, PhD thesis, Université de Nice–Sophia Antipolis, 2006, https://tel.archives-ouvertes.fr/tel-00141417v1.

[38] F. Malgouyres and F. Guichard, *Edge direction preserving image zooming: a mathematical and numerical analysis*, SIAM Journal on Numerical Analysis, 39 (2001), pp. 1–37 (electronic), https://doi.org/10.1137/S0036142999362286.

[39] E. Naden, T. März, and C. B. MacDonald, *Anisotropic diffusion filtering of images on curved surfaces*, tech. report, 2014, https://arxiv.org/abs/arXiv:1403.2131.

[40] P. Perona and J. Malik, *Scale-space and edge detection using anisotropic diffusion*, IEEE Transactions on pattern analysis and machine intelligence, 12 (1990), pp. 629–639, https://doi.org/10.1109/34.56205.

[41] A. Pressley, *Elementary differential geometry*, Springer Undergraduate Mathematics Series, Springer-Verlag London, Ltd., London, second ed., 2010, https://doi.org/10.1007/978-1-84882-891-9.

[42] U. Prüfert, F. Tröltzsch, and M. Weiser, *The convergence of an interior point method for an elliptic control problem with mixed control-state constraints*, Computational Optimization and Applications. An International Journal, 39 (2008), pp. 183–218, https://doi.org/10.1007/s10589-007-9063-7.

[43] P.-A. Raviart and J. M. Thomas, *A mixed finite element method for 2nd order elliptic problems*, in Mathematical aspects of finite element methods (Proc. Conf., Consiglio Naz. delle Ricerche (C.N.R.), Rome, 1975), Springer, Berlin, 1977, pp. 292–315. Lecture Notes in Math., Vol. 606.

[44] M. E. Rognes, D. A. Ham, C. J. Cotter, and A. T. T. McRae, *Automating the solution of PDEs on the sphere and other manifolds in FEniCS 1.2*, Geoscientific Model Development, 6 (2013), pp. 2099–2119, https://doi.org/10.5194/gmd-6-2099-2013.

[45] S. Rosenberg, *The Laplacian on a Riemannian Manifold*, vol. 31 of London Mathematical Society Students Texts, Cambridge University Press, 1997.

[46] L. I. Rudin, S. Osher, and E. Fatemi, *Nonlinear total variation based noise removal algorithms*,

Physica D, 60 (1992), pp. 259–268, https://doi.org/10.1016/0167-2789(92)90242-F.

[47] A. Schiela, *Barrier methods for optimal control problems with state constraints*, SIAM Journal on Optimization, 20 (2009), pp. 1002–1031, https://doi.org/10.1137/070692789.

[48] D. Strong and T. Chan, *Edge-preserving and scale-dependent properties of total variation regularization*, Inverse Problems. An International Journal on the Theory and Practice of Inverse Problems, Inverse Methods and Computerized Inversion of Data, 19 (2003), pp. S165–S187, https://doi.org/10.1088/0266-5611/19/6/059. Special section on imaging.

[49] M. Ulbrich and S. Ulbrich, *Primal-dual interior point methods for PDE-constrained optimization*, Mathematical Programming, 117 (2009), pp. 435–485, https://doi.org/10.1007/s10107-007-0168-7.

[50] D. Wachsmuth, *Numerical solution of optimal control problems with convex control constraints*, in Systems, control, modeling and optimization, vol. 202 of IFIP Int. Fed. Inf. Process., Springer, New York, 2006, pp. 319–327, https://doi.org/10.1007/0-387-33882-9_30.

[51] Y. Wang, J. Yang, W. Yin, and Y. Zhang, *A new alternating minimization algorithm for total variation image reconstruction*, SIAM Journal on Imaging Sciences, 1 (2008), pp. 248–272, https://doi.org/10.1137/080724265.

[52] C. Zălinescu, *Convex analysis in general vector spaces*, World Scientific Publishing Co., Inc., River Edge, NJ, 2002, https://doi.org/10.1142/9789812777096.

[53] W. P. Ziemer, *Weakly differentiable functions*, vol. 120 of Graduate Texts in Mathematics, Springer-Verlag, New York, 1989, https://doi.org/10.1007/978-1-4612-1015-3. Sobolev spaces and functions of bounded variation.